1521-009X/46/11/1756–1766$35.00
Drug Metabolism and Disposition

https://doi.org/10.1124/dmd.118.081216
Drug Metab Dispos 46:1756–1766, November 2018

Special Section – New Models in Drug Metabolism and Transport

Characterization of P-Glycoprotein Humanized Mice Generated by Chromosome Engineering Technology: Its Utility for Prediction of Drug Distribution to the Brain in Humans[S]

Yuki Yamasaki, Kaoru Kobayashi, Fuka Okuya, Naoyo Kajitani, Kanako Kazuki, Satoshi Abe, Shoko Takehara, Shingo Ito, Seiryo Ogata, Tatsuki Uemura, Sumio Ohtsuki, Genki Minegishi, Hidetaka Akita, Kan Chiba, Mitsuo Oshimura, and Yasuhiro Kazuki

Graduate School of Pharmaceutical Sciences, Chiba University, Chiba, Japan (Y.Y., K.Ko., F.O., G.M., H.A., K.C.); Chromosome Engineering Research Center (N.K., K.Ka., S.A., S.T., M.O., Y.K.) and Department of Biomedical Science, Institute of Regenerative Medicine and Biofunction, Graduate School of Medical Science (Y.K.), Tottori University, Tottori, Japan; and Department of Pharmaceutical Microbiology, Faculty of Life Sciences, Kumamoto University, Kumamoto, Japan (S.I., S.Og., T.U., S.Oh.)

Received March 4, 2018; accepted May 16, 2018

ABSTRACT

P-glycoprotein (P-gp), encoded by the *MDR1* gene in humans and by the *Mdr1a/1b* genes in rodents, is expressed in numerous tissues and performs as an efflux pump to limit the distribution and absorption of many drugs. Owing to species differences of P-gp between humans and rodents, it is difficult to predict the impact of P-gp on pharmacokinetics and the tissue distribution of P-gp substrates in humans from the results of animal experiments. Therefore, we generated a novel P-gp humanized mouse model by using a mouse artificial chromosome (MAC) vector [designated human MDR1-MAC (hMDR1-MAC) mice]. The results showed that hMDR1 mRNA was expressed in various tissues of hMDR1-MAC mice. Furthermore, the expression of human P-gp was detected in the brain capillary fraction and plasma membrane fraction of intestinal epithelial cells isolated from hMDR1-MAC mice, although the expression levels of intestinal P-gp were extremely low. Thus, we evaluated the function of human P-gp at the blood-brain barrier of hMDR1-MAC mice. The brain-to-plasma ratios of P-gp substrates in hMDR1-MAC mice were much lower than those in Mdr1a/1b-knockout mice, and the brain-to-plasma ratio of paclitaxel was significantly increased by pretreatment with a P-gp inhibitor in hMDR1-MAC mice. These results indicated that the hMDR1-MAC mice are the first P-gp humanized mice expressing functional human P-gp at the blood-brain barrier. This mouse is a promising model with which to evaluate species differences of P-gp between humans and mice in vivo and to estimate the brain distribution of drugs in humans while taking into account species differences of P-gp.

Introduction

P-glycoprotein (P-gp), the product of the *MDR1* (*ABCB1*) gene in humans and the *Mdr1a* and *Mdr1b* genes in rodents, is a member of the superfamily of ATP-binding cassette (ABC) transporters. P-gp serves to restrict the entry of compounds into tissues [e.g., blood-brain barrier (BBB)], to limit the absorption of compounds into systemic circulation (e.g., intestine) and to mediate elimination from the body (e.g., liver and kidney) (Ayrton and Morgan, 2001; Leslie et al., 2005; Callaghan et al., 2008; Hodges et al., 2011). Since P-gp exhibits a broad specificity in substrate recognition, P-gp can affect the pharmacokinetics of many drugs (Callaghan et al., 2008; Hodges et al., 2011; Silva et al., 2015).

On the basis of such clinical relevance, the Food and Drug Administration, the European Medicines Agency, and the International Transporter Consortium recommend that P-gp substrate or inhibition studies should be undertaken at the preclinical stage in drug development (Giacomini et al., 2010; European Medicines Agency, 2012; Food and Drug Administration, 2017). To clarify the impact of P-gp on a the disposition, efficacy, and safety of a drug, interactions of P-gp with

This work was supported in part by the Chiba University SEEDS Fund (Chiba University Open Recruitment for International Exchange Program), the Regional Innovation Strategy Support Program from the Ministry of Education, Culture, Sports, Science and Technology, the Funding Program for Next Generation World-Leading Researchers (NEXT Program) from the Japan Society for the Promotion of Science (Y.K.) [Grant number LS085], and the Basis for Supporting Innovative Drug Discovery and Life Science Research from the Japan Agency for Medical Research and Development (Y.K.) [Grant number JP17am0101124].
https://doi.org/10.1124/dmd.118.081216.
[S]This article has supplemental material available at dmd.aspetjournals.org.

ABBREVIATIONS: ABC, ATP-binding cassette; AUC, area under the curve; BBB, blood-brain barrier; BCRP, breast cancer resistance protein; CHO, Chinese hamster ovary; ES, embryonic stem; FBS, fetal bovine serum; FISH, fluorescence in situ hybridization; GAPDH, glyceraldehyde-3-phosphate dehydrogenase; hChr.7, human chromosome 7; hMDR1, human MDR1; HPRT, 3′hypoxanthine-guanine phosphoribosyl transferase; KO, knockout; $K_{p,brain}$, ratio of $AUC_{brain\ (0–2\ hour)}$ to $AUC_{brain\ (0–2\ hour)}$; LC-MS/MS, liquid chromatography-tandem mass spectrometry; MAC, mouse artificial chromosome; MEF, mouse embryonic fibroblast; MMCT, microcell-mediated chromosome transfer; PCR, polymerase chain reaction; P-gp, P-glycoprotein; PXR, pregnane X receptor; RT, reverse transcription; SNP, single-nucleotide polymorphism; Tc, transchromosomic, WT, wild-type.

substrates and inhibitors have been investigated by in vitro bidirectional transporter assays using Caco-2 or P-gp–overexpressing cell lines (Giacomini et al., 2010; European Medicines Agency, 2012; Food and Drug Administration, 2017). Recent studies have suggested that a combination of studies using P-gp–overexpressing cells with a protein quantification method is a useful in vitro-to-in vivo translational model with which to predict brain penetration of P-gp substrates (Uchida et al., 2011a, 2014). However, it still remains challenging to predict the involvement of human P-gp in pharmacokinetics in vivo from in vitro data.

P-gp-knockout (KO) mice and rats have been used for in vivo study to determine the impact of P-gp on the pharmacokinetics and tissue distribution of various P-gp substrates (Schinkel et al., 1994, 1997; Chu et al., 2012). On the other hand, several studies have demonstrated the existence of species differences of P-gp between humans and rodents, which limit the use of these KO animals. The species differences of P-gp include differences in expression level and substrate specificity. For instance, P-gp expression levels in human brain capillaries were shown to be approximately 3-fold lower than those in mouse brain capillaries (Uchida et al., 2011b; Chu et al., 2013). In addition, P-gp substrate specificity is different in humans and mice (Yamazaki et al., 2001; Takeuchi et al., 2006; Baltes et al., 2007), though there are some contradictory results showing few differences in P-gp substrate susceptibility (Feng et al., 2008). One of the reasons why the species differences associated with P-gp are still controversial is that there is no appropriate tool to evaluate the differences except for cell lines.

To predict the involvement of transporters in the pharmacokinetics in humans in vivo, the development of humanized mouse models is a valuable approach that can overcome the problem of species differences between humans and mice. Regarding other members of the superfamily of ABC transporters, humanized mouse models for multidrug resistance protein 2 and breast cancer resistance protein (BCRP) have already been generated (Scheer et al., 2012; Dallas et al., 2016). Following this strategy, Sadiq et al. (2015) first reported the generation of P-gp humanized mice. However, the mice were determined to be "insufficient humanized mice" since P-gp expressed at the BBB of humanized mice was not functional. Thus, the generation of a P-gp humanized mouse model that expresses "functional" P-gp is still needed.

In this study, we generated a novel P-gp humanized mouse model using mouse artificial chromosome (MAC) vectors with chromosome-engineering techniques [designated human MDR1-MAC (hMDR1-MAC) mice]. The MAC vector exhibits several important characteristics that are desirable for ideal gene-delivery vectors. These characteristics include stable episomal maintenance and the capacity to carry large genomic loci with their regulatory elements, thereby allowing physiologic regulation of the introduced gene in a manner similar to that of the native chromosome (Oshimura et al., 2015; Satoh et al., 2018). Furthermore, we evaluated the expression of hMDR1 mRNA and human P-gp in the tissues of hMDR1-MAC mice. Since the expression level of human P-gp in the isolated brain capillary fraction was substantial, we evaluated the function of human P-gp expressed at the BBB of hMDR1-MAC mice. In addition, we assessed the usefulness of hMDR1-MAC mice as a tool for predicting the impact of human P-gp at the BBB on the brain distribution of drugs and for evaluating the species differences of P-gp between humans and mice in vivo.

Materials and Methods

Plasmid Construction

Targeting vectors were constructed as follows. For pAC005045-loxP-BS, two 2.5- and 5.3-kb fragments for homologous arms, corresponding to AC005045, were amplified by polymerase chain reaction (PCR) using primers hMDR1loxP2L/hMDR1loxP1R (~8.6 kb). The PCR product was digested with BglII, and the 2.5- and 5.3-kb fragments were subcloned into BglII and BamHI of the pKO Scrambler V901 backbone vector, respectively (Lexicon Genetics, Woodlands, TX). The loxP cassette containing CMV-BS, loxP, and 3′hypoxanthine-guanine phosphoribosyl transferase (HPRT) was cloned into a vector into which the homologous arms had been inserted. For pBS-TEL/AC003083Puro, a PCR product from AC003083 was amplified by PCR primers hMDR1tel5L/hMDR1tel5R (7.5 kb), digested with EcoRI/PstI, and subcloned into EcoRI/PstI sites of the pBS-TEL/Puro vector (Kazuki et al., 2013).

Cell Culture

hMDR1-MAC was constructed using a previously described Mb-sized gene cloning system via MAC (Y. Kazuki, K. Kobayashi, M. Hirabayashi, S. Abe, N. Kajitani, K. Kazuki, S. Takehara, M. Takiguchi, D. Satoh, J. Kuze, T. Sakuma, T. Kaneko, T. Mashimo, M. Osamura, M. Hashimoto, R. Wakatsuki, R. Hirashima, R. Fujiwara, T Deguchi, A. Kurihara, Y. Tsukazaki, N. Senda, T. Yamamoto, N. Scheer, and M. Oshimura, submitted manuscript). The MAC4 vector was used to generate hMDR1-MAC. The structure of MAC4 contained a centromere from mouse chromosome 11, enhanced green fluorescent protein flanked by HS4 insulators, 5′HPRT-loxP site, PGKhyg, PGKpuro, and telomeres (unpublished data). Chicken DT40 cells containing human chromosome 7 (hChr.7) were maintained at 40°C in RPMI 1640 supplemented with 10% fetal bovine serum (FBS; Hyclone Laboratories, Logan, UT), 1% chicken serum, 50 μM 2-mercaptoethanol, and 1.5 mg/ml G418. Hprt-deficient Chinese hamster ovary [CHO ($Hprt^{-/-}$)] cells containing MAC4 used as fusion recipients for hChr.7 transfer were maintained at 37°C in Ham's F-12 medium nutrient mixture (Invitrogen, Carlsbad, CA) supplemented with 10% bovine calf serum. Mouse embryonic fibroblasts (MEFs) were isolated from Jcl:ICR (CLEA Japan, Tokyo, Japan) embryos at 13.5 days postcoitum. MEFs were grown in Dulbecco's modified Eagle's medium (Sigma-Aldrich, St. Louis, MO) plus 10% FBS. Parental mouse embryonic stem (ES) cell lines, TT2F, and microcell hybrid TT2F clones were maintained on mitomycin C (Sigma-Aldrich)–treated MEFs as feeder layers in Dulbecco's modified Eagle's medium with 18% FBS, 1 mM sodium pyruvate (Invitrogen), 0.1 mM nonessential amino acids (Invitrogen), 0.1 mM 2-mercaptoethanol (Sigma-Aldrich), 2 mM L-glutamine (Invitrogen), and 1000 U/ml leukemia inhibitory factor (Funakoshi, Tokyo, Japan).

Modification of hChr.7 in DT40 Cells

Homologous recombination-proficient chicken DT40 cells (1×10^7) were collected in 0.5 ml of RPMI with 25 μg of a linearized targeting vector and electroporated at 550 V and 25 μF using a Gene Pulser apparatus (Bio-Rad, Hercules, CA). Drug-resistant DT40 clones were selected in 1.5 mg/ml G418, 0.3 μg/ml puromycin, or 15 μg/ml blasticidin S. Homologous recombination in DT40 hybrid clones was identified by PCR analyses as follows.

Microcell-Mediated Chromosome Transfer

Microcell-mediated chromosome transfer (MMCT) was performed as described previously (Kazuki et al., 2013). DT40 cells containing the modified chromosomes (hChr.7-loxP-ΔAC003083) were transferred to CHO cells (MAC4) via MMCT. To transfer hMDR1-MAC to mouse ES cells, CHO cells, or A9 cells containing the hMDR1-MAC were used as donor microcell hybrids. Briefly, mouse ES cells were fused with microcells prepared from the donor hybrid cells and selected with puromycin (0.75 μg/ml). The transferred hMDR1-MAC was characterized by PCR and fluorescence in situ hybridization (FISH) analyses.

FISH Analyses

Trypsinized cells were incubated for 15 minutes in 75 mM KCl and fixed with methanol and acetic acid (3:1), and then slides were prepared using standard methods. FISH analyses were performed using fixed metaphase or interphase spreads of each cell hybrid with digoxigenin-labeled (Roche, Basel, Switzerland) DNA [human COT-1 DNA, mouse COT-1 DNA (Invitrogen), mouse minor satellite DNA (a gift from Dr. Vladimir Larionov, Head Investigator, Institution; National Cancer Institute, Developmental Therapeutics Branch, Bethesda, MD 20892, USA)] and biotin-labeled DNA [MDR1-BAC (RP11-784L5), mouse COT-1 DNA, CMV-BS, and PGK-Puro], essentially as described previously (Kazuki et al., 2013). Chromosomal DNA was counterstained with 4′,6-diamidino-2-phenylindole (Sigma-Aldrich). Images were captured using the NIS-Elements system (Nikon, Tokyo, Japan) or an AxioImagerZ2 Fluorescence Microscope (Carl Zeiss, Oberkochen, Germany).

Generation of Transchromosomic Mice

Chimeric mice were produced from two TT2F (hMDR1-MAC) cell lines for the transchromosomic (Tc) line. Chimera production was completed as described previously (Kazuki et al., 2013). Briefly, ES cells were injected into eight cell–stage embryos derived from ICR mice (CLEA Japan) and then transferred into pseudopregnant ICR females. Three chimeric mice with 80%–100% coat-color chimerism were used to generate mice in which germline transmission could successfully occur in each line. Such mice were further mated with Mdr1a/b-KO mice to generate fully humanized hMDR1 mice (designated hMDR1-MAC mice). Male ICR [wild-type (WT); CLEA Japan], Mdr1a/b-KO (Taconic Farms, Germantown, NY), and hMDR1-MAC mice (9–12 weeks old) were used for the experiments. All of the mice were maintained under a standard 12-hour light/dark cycle, with water and chow provided ad libitum. All animal studies were conducted in accordance with the guidelines for the Care and Use of Laboratory Animals adopted by the Committee on Animal Research of Chiba University and Tottori University.

Genomic PCR Analyses

Genomic DNA was extracted from cell lines and from Tc mouse tissue specimens using a genomic extraction kit (Gentra System, Minneapolis, MN). PCR was performed using the primers shown in Supplemental Table 1.

Reverse-Transcription PCR Analyses

Total RNAs from the tissues of hMDR1-MAC mice were prepared using ISOGEN II (Nippon Gene, Tokyo, Japan) in accordance with manufacturer instructions. Genomic DNA was eliminated by treatment with recombinant RNase-free DNase I (Roche). First-strand cDNA was generated with random hexamer primers and High-Capacity cDNA Reverse Transcription (RT) Kits (Applied Biosystems, Foster City, CA). The expression of hMDR1 was detected using TaqMan Gene Expression Assays (catalog number Hs00184500_m1; Applied Biosystems) and THUNDERBIRD Probe qPCR Mix (TOYOBO, Osaka, Japan). The expression of mouse glyceraldehyde-3-phosphate dehydrogenase (GAPDH) was detected using specific primers (forward, 5′-AAGCCCATCACCATCTTCCAGG-3′; reverse, 5′-GGTTCACACCCATCACAAACAT-3′) and EmeraldAmp MAX PCR Master Mix (TaKaRa Bio Inc., Kusatsu, Japan). Amplifications were performed under the conditions shown in Supplemental Table 2. Amplified fragments were then resolved by electrophoresis on 3.5% Agarose SFR (Amresco, Solon, OH) gel and 3% standard agarose (Nippon Gene) gel for the detection of hMDR1 and GAPDH, respectively, followed by staining with ethidium bromide.

Quantification of Protein Expression Levels in Brain Capillaries and Plasma Membrane Fractions of Small Intestinal Epithelial Cells

Isolation of Mouse Brain Capillaries. Brain capillaries of WT, Mdr1a/1b-KO, and hMDR1-MAC mice were isolated from pooled frozen brains (10 mice/group), as described previously (Uchida et al., 2013) with minor modification. Briefly, the brain homogenate was centrifuged with dextran to concentrate brain capillaries. Brain capillaries were further purified by filtration through nylon meshes (210, 85, and 45 μm) and were collected on 20-μm nylon meshes. The isolated brain capillary fractions were lysed in a hypotonic buffer by sonication, and protein concentration was measured with a Pierce BCA Protein Assay Kit (Thermo Fisher Scientific, Lafayette, CO).

Isolation of Plasma Membrane Fractions of Mouse Small Intestinal Epithelial Cells. The plasma membrane fractions of intestinal epithelial cells were isolated from pooled small intestines of WT, Mdr1a/1b-KO, and hMDR1-MAC mice (five mice/group). Each mouse was slaughtered by cervical dislocation, and the duodenum (first 5 cm from the pylorus) was removed. Fragments of the duodenum were cut into 1-cm pieces, incised, and then pooled for each group. Subsequent preparation was performed as described previously (Akazawa et al., 2016). Protein concentrations were measured by the Lowry method using DC Protein Assay Reagent (Bio-Rad).

Multiplexed Multiple Reaction Monitoring Analysis. Protein expression amounts of the target molecules were simultaneously determined by multiplexed multiple reaction monitoring analysis, as described previously (Uchida et al., 2013; Nakamura et al., 2016). Briefly, the protein samples were denatured with 12 mM sodium deoxycholate and 12 mM *N*-lauroylsarcosinate, and were digested by lysyl endopeptidase and trypsin after reduction and alkylation (Masuda et al., 2008). Stable isotope-labeled peptides were spiked in the digested peptide samples as internal standards. Then the peptide samples were desalted and dissolved in 0.1% formic acid for liquid chromatography in combination with tandem mass spectrometry (LC-MS/MS) analysis. Standard samples were prepared as a single dilution series of unlabeled standard peptides at injection amounts (0.5–100 fmol) with 30 fmol of internal standard peptides. The samples were analyzed by using a micro-LC system with a ChromXP C18CL Column (Ekisigent, Redwood City, CA) coupled to an electrospray ionization triple-quadrupole mass spectrometer (QTRAP6500; SCIEX, Framingham, MA). The transitions are listed in Supplemental Table 3. The data were analyzed by MultiQuant3 (SCIEX). The quantification value was determined as the average value of the peak ratios from three to four sets of transitions.

Study Design for In Vivo Experiments

Preparation of Drug Solutions. Elacridar hydrochloride was purchased from Axon Medchem (Groningen, The Netherlands). Indinavir sulfate was purchased from Cayman Chemicals (Ann Arbor, MI). Hydroxyzine hydrochloride was purchased from Wako Pure Chemicals (Osaka, Japan). Loperamide hydrochloride, quinidine sulfate, ritonavir, and verapamil hydrochloride were purchased from Tokyo Chemical Industry (Tokyo, Japan). Paclitaxel was purchased from KareBay Biochem (Monmouth Junction, NJ). Vinblastine sulfate was purchased from Sigma-Aldrich.

Stock solutions of paclitaxel (6 mg/ml) and ritonavir (3 mg/ml) were made in ethanol and Tween 80 (1:1, v/v). Before administration, the stock solutions were diluted further with sterile saline to final concentrations of 1.5 and 0.75 mg/ml, respectively. A suspension of elacridar (5 mg/ml) was made in water and concentrated stock [10 g/l hydroxypropyl methyl cellulose (Shin-Etsu Chemical, Tokyo, Japan) and 2% Tween 80 in water, 1:1, v/v]. The solutions of other drugs were made in sterile saline at concentrations of 0.5 mg/ml for hydroxyzine hydrochloride and indinavir sulfate, 0.2 mg/ml for loperamide hydrochloride, 1 mg/ml for quinidine sulfate, 0.1 mg/ml for verapamil hydrochloride, and 0.4 mg/ml for vinblastine sulfate.

Brain Penetration Study. WT, Mdr1a/1b-KO, and hMDR1-MAC mice ($n = 3$–6/time point) were intravenously administered hydroxyzine hydrochloride (5 mg/kg), indinavir sulfate (5 mg/kg), loperamide hydrochloride (2 mg/kg), paclitaxel (10 mg/kg), quinidine sulfate (10 mg/kg), ritonavir (5 mg/kg), verapamil hydrochloride (1 mg/kg), or vinblastine sulfate (4 mg/kg). The drugs were injected via the tail vein in a volume of 6.7 ml/kg b.wt. for paclitaxel and 10 ml/kg b.wt. for other drugs. Mice were sacrificed by cervical dislocation at 0.5–4 hours after administration of the drugs, and blood was collected from the postcaval vein and immediately centrifuged at 10,000*g* for 10 minutes to obtain plasma. The brain of each mouse was also removed and weighed and then homogenized in four volumes (w/v) of water. All samples were stored at −80°C until preparation for LC-MS/MS analysis.

P-gp Inhibition Study. hMDR1-MAC mice (n = 4/group) were orally administered a vehicle (water and concentrated stock, 1:1, v/v) or 50 mg/kg elacridar (10 ml/kg b.wt.). At 4 hours after administration of elacridar, mice were intravenously administered 10 mg/kg paclitaxel (6.7 ml/kg b.wt.) in the tail vein. Mice were sacrificed by cervical dislocation at 4 hours after administration of paclitaxel, and plasma and the brain were collected as described above.

Quantification of Drugs in Plasma and the Brain

Plasma and brain homogenates were prepared as described in Supplemental Materials and Methods and were used for LC-MS/MS analysis. The LC-MS/MS conditions are shown in Supplemental Materials and Methods and Supplemental Table 4.

Data and Statistical Analyses

The values of the area under the curve (AUC) were calculated using the trapezoid rule. The values of $K_{p,brain}$ were obtained from the ratio of $AUC_{brain\ (0–2\ hour)}$ to $AUC_{plasma\ (0–2\ hour)}$. The $K_{p,brain}$ ratio was determined as ($K_{p,brain}$ in Mdr1a/1b-KO mice)/($K_{p,brain}$ in WT or hMDR1-MAC mice). The values of transport activity per P-gp molecule, which was defined in a previous report (Uchida et al., 2014), were calculated as [($K_{p,brain}$ ratio) − 1]/[P-gp expression levels in brain capillaries of WT and hMDR1-MAC mice].

Data are presented as the mean ± S.D. or S.E.M. Statistical analyses were performed using Statcel (OMS, Tokyo, Japan). Comparison of multiple groups was made by analysis of variance followed by the post hoc test of Scheffé's F test. Comparison of two groups was made with Welche's t-test. $P < 0.05$ was considered statistically significant.

Results

Generation of hMDR1-MAC Mice. The hMDR1-MAC was constructed via Cre-loxP–mediated chromosomal translocation, as described previously (Kazuki et al., 2013; Takiguchi et al., 2014). To clone ~210 kb of the *hMDR1* gene on hChr.7 into a modified MAC (MAC4), a loxP sequence was introduced to the AC005045 locus on hChr.7, and the hChr.7 was truncated at the AC003083 locus in DT40 cells (Supplemental Fig. 1). With the targeting construct pAC005045-loxP-BS for the cloning site (loxP) and positive selection (blasticidin S), three of nine drug-resistant clones selected in the presence of G418 and blasticidin S were targeted correctly, as shown by PCR (designated hChr.7-loxP) (data not shown). FISH analyses showed that the targeting construct was integrated into the correct locus on hChr.7-loxP in DT40 cells (data not shown). With the targeting construct pBS-TEL/AC003083Puro, for telomere-associated chromosomal truncation at the AC003083 locus on hChr.7 (Supplemental Fig. 2), 3 of 96 drug-resistant clones selected in the presence of puromycin were targeted correctly, as shown by PCR (designated hChr.7-loxP-ΔAC003083) (data not shown). FISH analyses showed that the targeting construct was integrated into the correct locus on hChr.7 in DT40 cells (data not shown). hChr.7-loxP-ΔAC003083 in DT40 (hChr.7-loxP-ΔAC003083) cells was then introduced into CHO cells containing a MAC vector (MAC4 with hygromycin-resistant gene, enhanced green fluorescent protein, and loxP) using MMCT to obtain hybrid CHO clones with two different exogenous chromosomes: the MAC4 and the modified hChr.7 (hChr.7-loxP-ΔAC003083). To induce reciprocal translocation between the MAC4 and the modified hChr.7, Cre expression vectors were transfected to the CHO hybrids, and recombinant clones were selected using hypoxanthine-aminopterin-thymidine medium over a period of 10 days (Supplemental Fig. 3). Six of 10 drug-resistant clones were PCR positive with hMDR1, MAC, and HPRT gene reconstitution–specific primers. FISH analyses showed that the defined region of hChr.7 containing the *hMDR1* gene was cloned into the MAC4 vector in CHO hybrid cells (designated hMDR1-MAC) (Fig. 1).

hMDR1-MAC was introduced into a mouse ES cell line (TT2F) via CHO or A9 cells using MMCT as shown in Supplemental Fig. 4A. PCR analyses using primers for the detection of the hMDR1-MAC showed that two of five mouse ES (hMDR1-MAC) clones contained intact hMDR1-MAC (data not shown). FISH analyses showed that the hMDR1-MAC was present as an individual chromosome without integration into the host mouse chromosomes in these mouse ES cells (Supplemental Fig. 4B). Two mouse ES (hMDR1-MAC) clones that were karyotypically normal were used for subsequent production of chimeras. Chimeric mice were produced from the ES lines, and chimeras with various forms of coat-color chimerism were successfully obtained. The germline transmission was confirmed by PCR analyses in offspring from the three chimeric mice with 80%–100% coat-color chimerism. The littermates were further mated with WT mice to generate Tc mice with the hMDR1-MAC. The Tc mice were further mated with Mdr1a/1b-KO mice to generate fully humanized MDR1 mice (designated hMDR1-MAC mice). The hMDR1-MAC mice were healthy and showed no obvious phenotypic abnormalities.

Expression of hMDR1 mRNA in Various Tissues of hMDR1-MAC Mice. To confirm the expression of hMDR1 mRNA in hMDR1-MAC mice, RT-PCR analysis was performed in various tissues of hMDR1-MAC mice. The expression of hMDR1 mRNA was detected in the brain, intestine, liver, kidney, spleen, adrenal gland, testis, stomach, thymus, and heart of hMDR1-MAC mice (Fig. 2). The expression of hMDR1 mRNA was not detected in the tissues of Mdr1a/1b-KO mice (data not shown).

Expression of P-gp. To determine the expression of P-gp in brain capillaries isolated from WT, Mdr1a/1b-KO, and hMDR1-MAC mice, LC-MS/MS analysis was carried out using peptides specific to human MDR1, mouse Mdr1a, and Mdr1b as well as peptides that are common to both human and mouse MDR1/Mdr1a. The recovered amounts of brain capillary fractions isolated from WT, Mdr1a/1b-KO, and hMDR1-MAC mice were 149, 230, and 204 μg of protein, respectively. In hMDR1-MAC mice, the expression levels of plasma membrane protein

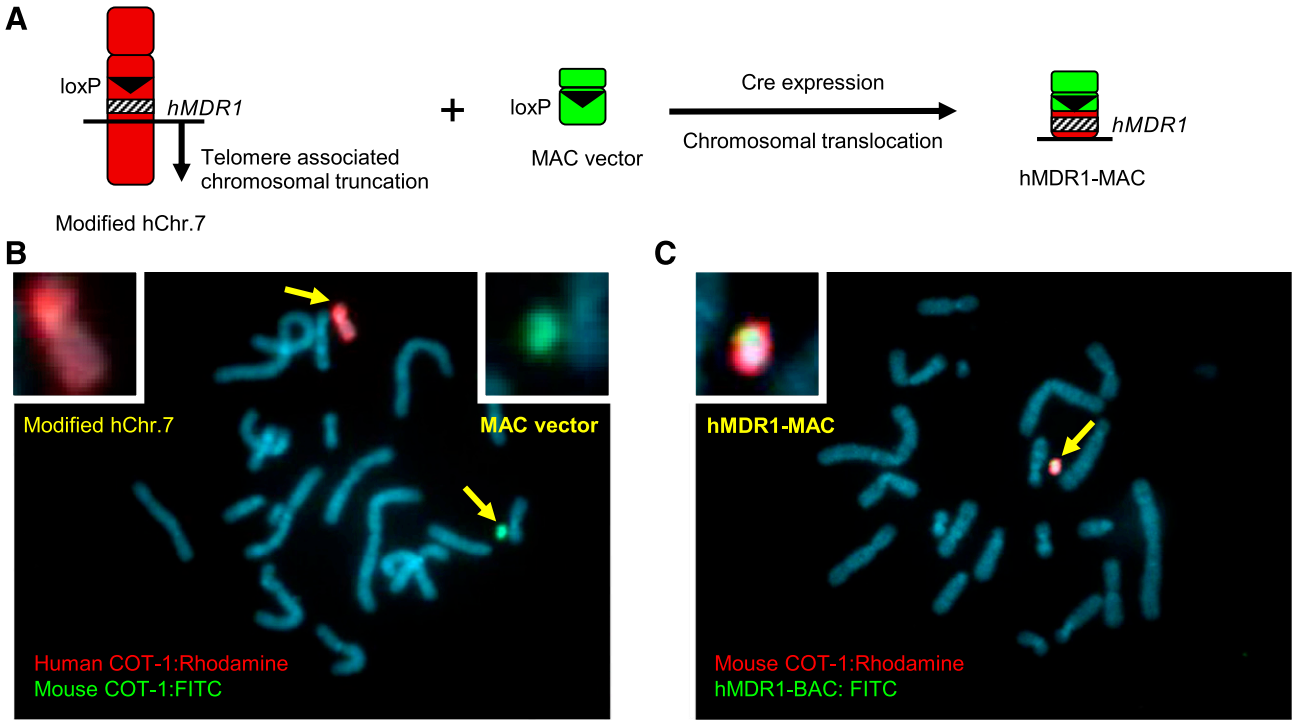

Fig. 1. Construction of hMDR1-MAC. (A) Schematic diagram of the construction of hMDR1-MAC. The *hMDR1* gene was cloned into the MAC vector via Cre-loxP–mediated chromosomal translocation. FISH images of CHO cells carrying modified hChr.7 and MAC (B) and CHO cells carrying hMDR1-MAC (C). Arrows indicate each chromosome. Insets show large images of each chromosome.

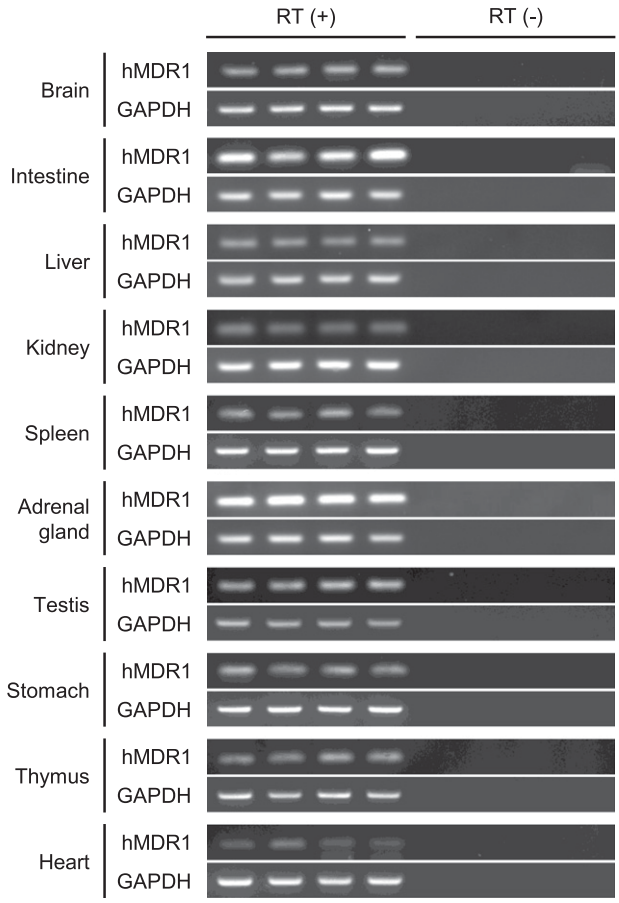

Fig. 2. Expression of hMDR1 mRNA in various tissues of hMDR1-MAC mice. RT-PCR analysis was performed for detection of hMDR1 mRNA in various tissues of hMDR1-MAC mice. Each lane represents samples from an individual mouse. The expression of mouse GAPDH was used as an internal control.

(Na^+/K^+-ATPase), which reflect the purity and homogeneity of brain capillaries in the isolated fraction (Uchida et al., 2011b), were 1.7-fold higher than those in WT mice (Table 1). A similar tendency was observed for ABC transporters (Mrp4 and Bcrp). As shown in Table 1, the peptides specific to human MDR1 and mouse Mdr1 were not detected in the isolated brain capillary fraction of Mdr1a/1b-KO mice. On the other hand, the peptide specific to human MDR1 was detected in the brain capillary fraction of hMDR1-MAC mice but not in those of WT mice, whereas the opposite was the case for mouse Mdr1-specific peptides (Table 1). For direct comparison of protein amounts in WT and hMDR1-MAC mice, we used data obtained with the common MDR1/Mdr1a peptide (Table 1). Expression of MDR1/Mdr1a protein was observed in both WT and hMDR1-MAC mice. The amount of MDR1/Mdr1a protein in hMDR1-MAC mice was 0.43-fold smaller than that in WT mice (2.21 vs. 5.15 fmol/μg of protein).

In addition to brain capillaries, we isolated the plasma membrane fraction of intestinal epithelial cells from WT, Mdr1a/1b-KO, and hMDR1-MAC mice to determine the expression of P-gp using LC-MS/MS. The recovered amounts of the plasma membrane fractions of intestinal epithelial cells isolated from WT, Mdr1a/1b-KO, and hMDR1-MAC mice were 760, 941, and 679 μg of protein, respectively. As shown in Supplemental Table 5, no significant differences in Na^+/K^+-ATPase expression levels, which reflect the purity and homogeneity of the plasma membrane fraction of intestinal epithelial cells (Akazawa et al., 2016), were observed between WT and hMDR1-MAC mice, suggesting no differences in the purity and homogeneity between WT and hMDR1-MAC mice. The peptides specific to human MDR1 and mouse Mdr1 were not detected in the plasma membrane fraction of intestinal epithelial cells of Mdr1a/1b-KO mice (Supplemental Table 5), which is consistent with the results for brain capillaries. Furthermore, the peptide specific to human MDR1 was detected in intestinal epithelial cells of hMDR1-MAC mice but not in those of WT mice, whereas the opposite was the case for mouse Mdr1-specific peptides (Supplemental Table 5). Expression of MDR1/Mdr1a protein was observed in both WT and hMDR1-MAC mice. The amount of MDR1/Mdr1a protein in hMDR1-MAC mice was 0.03-fold smaller than that in WT mice (0.70 vs. 22.86 fmol/μg of protein).

Function of P-gp at the BBB. Since the expression level of P-gp in brain capillaries of hMDR1-MAC mice was comparable to that in brain capillaries of WT mice, we then assessed the function of P-gp at the BBB by comparing the concentrations of paclitaxel, a representative substrate of P-gp, in the brain and plasma of WT, Mdr1a/1b-KO, and hMDR1-MAC mice. After intravenous administration of paclitaxel, the brain concentration of paclitaxel in Mdr1a/1b-KO mice was markedly higher than the concentrations in WT and hMDR1-MAC mice (8.5-fold and 11.6-fold higher, respectively) (Fig. 3A), though no significant

TABLE 1

Protein expression levels of membrane proteins in isolated brain capillary fraction of WT, Mdr1a/1b-KO, and hMDR1-MAC mice

Brain capillary fractions were prepared from pooled frozen brains of WT, Mdr1a/1b-KO, and hMDR1-MAC mice (10 mice/group), and the protein expression levels were quantified by LC-MS/MS. The protein expression levels in four sets of transitions in one pooled sample from 10 mice were used to calculate the average (mean) and variability (S.E.M.), which are shown as the mean ± S.E.M. Peak area ratio was lower than the lowest point of the standard curve (0.5 fmol/5 μg of protein).

Molecular Names	Protein Expression Level		
	WT Mice	Mdr1a/1b-KO Mice	hMDR1-MAC Mice
		(*fmol/μg of protein*)	
Human MDR1 and Mouse Mdr1a[a]	5.15 ± 0.62	ULQ (<0.10)	2.21 ± 0.19*
Human MDR1[b]	ULQ (<0.10)	ULQ (<0.10)	2.77 ± 0.05
Mouse Mdr1a[c]	4.30 ± 0.21	ULQ (<0.10)	ULQ (<0.10)
Mouse Mdr1b	ULQ (<0.10)	ULQ (<0.10)	ULQ (<0.10)
Mrp4	0.54 ± 0.01	0.51 ± 0.02	0.89 ± 0.02*
Bcrp	2.24 ± 0.09	2.61 ± 0.12	3.61 ± 0.15*
Na^+, K^+-ATPase	66.75 ± 3.41	153.18 ± 6.63*	116.43 ± 3.09*

ULQ, under the limit of quantification.
[a]Measured by using a peptide probe set common for human MDR1 and mouse Mdr1a.
[b]Measured by using a peptide probe set specific for human MDR1.
[c]Measured by using a peptide probe set specific for mouse Mdr1a.
*$P < 0.01$, significantly different from the protein expression amounts in brain capillaries isolated from WT mice.

difference was observed among the three lines in plasma concentrations of paclitaxel (Fig. 3B). The brain-to-plasma ratio of paclitaxel in Mdr1a/1b-KO mice was also significantly higher than the ratios in WT and hMDR1-MAC mice (4.3-fold and 6.1-fold higher, respectively) (Fig. 3C), reflecting the difference in brain concentrations.

Next, to assess the possibility of inhibiting P-gp activity expressed in brain capillaries, we examined the effect of elacridar, a specific P-gp inhibitor, on the brain penetration of paclitaxel in hMDR1-MAC mice. Mice were administered elacridar orally at 4 hours before the administration of paclitaxel and then were administered paclitaxel

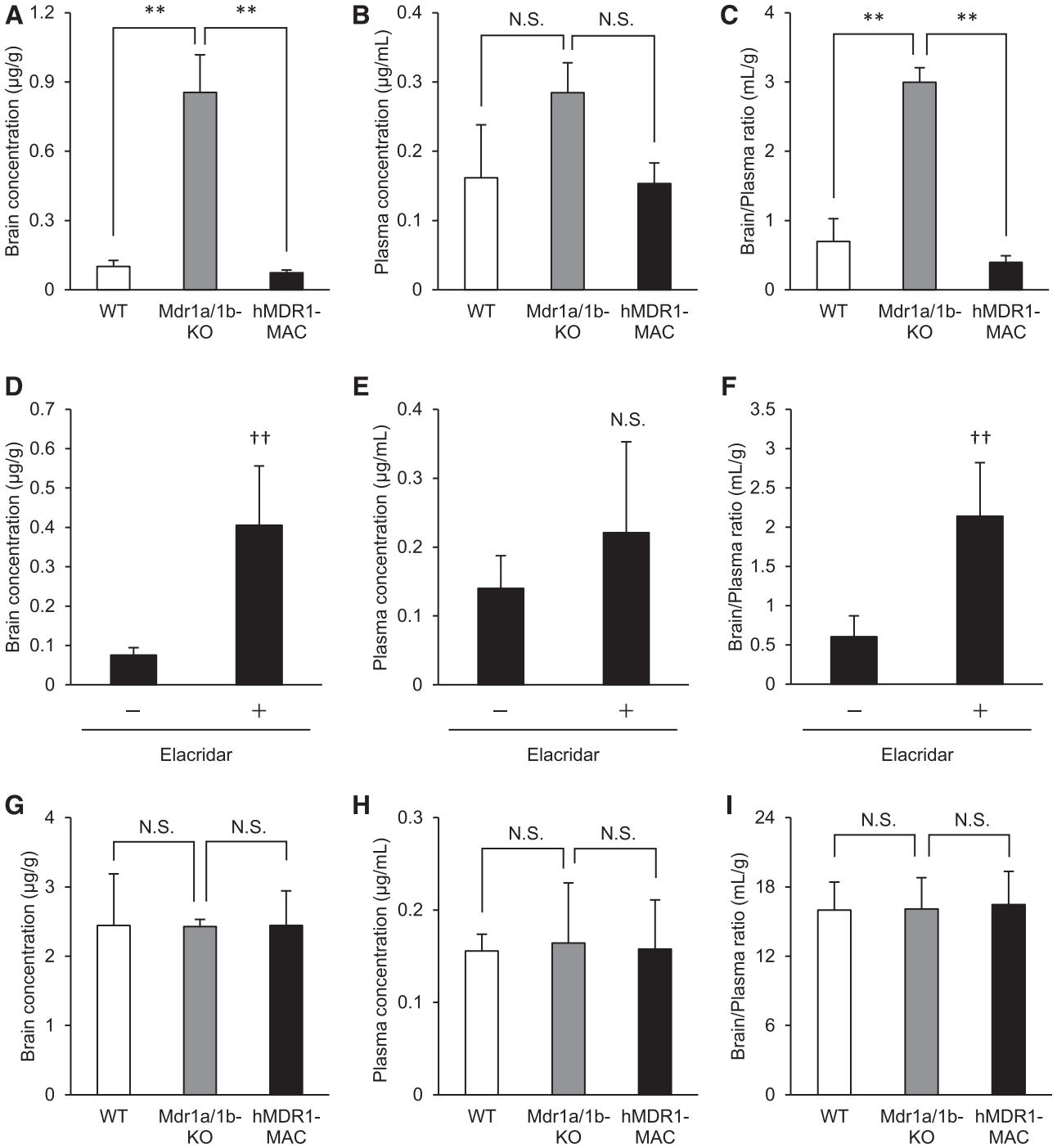

Fig. 3. Function of P-gp at the BBB of hMDR1-MAC mice. (A–C) Brain penetration of paclitaxel in WT, Mdr1a/1b-KO, and hMDR1-MAC mice. Mice (n = 3–4/group) were administered paclitaxel (10 mg/kg, i.v.) through the tail vein. Brains and plasma were collected at 4 hours after paclitaxel administration. (D–F) Effect of elacridar on brain penetration of paclitaxel in hMDR1-MAC mice. Mice (n = 4/group) were administered a solvent (vehicle) or elacridar (50 mg/kg, p.o.). At 4 hours after the administration of elacridar, mice were administered paclitaxel (10 mg/kg, i.v.) through the tail vein. Brains and plasma were collected at 4 hours after paclitaxel administration. (G–I) Brain penetration of hydroxyzine in WT, Mdr1a/1b-KO, and hMDR1-MAC mice. Mice (n = 3/group) were administered hydroxyzine hydrochloride (5 mg/kg, i.v.) through the tail vein. Brains and plasma were collected at 1 hour after hydroxyzine administration. Concentrations of paclitaxel and hydroxyzine in brains and plasma were determined by LC-MS/MS, each performed in duplicate. Brain concentrations (A, D, and G), plasma concentrations (B, E, and H), and brain-to-plasma ratios (C, F, and I) of paclitaxel or hydroxyzine. Data are shown as the mean ± S.D. of three or four mice. $^{**}P < 0.01$ compared with Mdr1a/1b-KO mice. $^{††}P < 0.01$ compared with vehicle-treated mice.

intravenously. As shown in Fig. 3D, the brain concentration of paclitaxel was increased by pretreatment with elacridar (5.4-fold), though the plasma concentration was not significantly changed (Fig. 3E). The brain-to-plasma ratio of paclitaxel was also significantly increased by pretreatment with elacridar (3.5-fold) (Fig. 3F), reflecting the difference in brain concentrations.

Furthermore, to confirm whether there are differences in the function of the BBB except for P-gp among WT, Mdr1a/1b-KO, and hMDR1-MAC mice, we assessed the brain penetration of hydroxyzine, which is a nonsubstrate of P-gp and crosses the BBB (Chen et al., 2003; Feng et al., 2008), in the three lines. After intravenous administration of hydroxyzine, no significant differences were observed among WT, Mdr1a/1b-KO, and hMDR1-MAC mice in brain and plasma concentrations of hydroxyzine (Fig. 3, G and H). Consequently, there was also no significant difference among the three lines in the brain-to-plasma concentration ratio of hydroxyzine (Fig. 3I).

Brain Penetration of Various P-gp Substrates. We also assessed the function of P-gp at the BBB by comparing the concentration-time profiles of various P-gp substrates in the brain and plasma among WT, Mdr1a/1b-KO, and hMDR1-MAC mice. Mice were intravenously administered indinavir, loperamide, paclitaxel, quinidine, ritonavir, verapamil, and vinblastine, and brain and plasma concentrations of the drugs were measured at 0.5-, 1-, or 2-hour time points. As shown in Fig. 4, the brain concentrations of all of the drugs tested were markedly higher in Mdr1a/1b-KO mice than in WT and hMDR1-MAC mice. On the other hand, Mdr1a/1b-KO mice showed no statistically significant difference in plasma concentrations of the drugs compared with the plasma concentrations in WT and hMDR1-MAC mice except for loperamide, paclitaxel, ritonavir, and vinblastine at some time points. The brain-to-plasma ratios were significantly higher in Mdr1a/1b-KO mice than in WT and hMDR1-MAC mice except for the 1-hour time point after the administration of ritonavir. The precise values of brain concentrations, plasma concentrations, and brain-to-plasma ratios are shown in Supplemental Table 6. As expected from these results, the values of $K_{p,brain}$ calculated from $AUC_{plasma\ (0–2\ hour)}$ and $AUC_{brain\ (0–2\ hour)}$ were markedly higher in Mdr1a/1b-KO mice than in WT and hMDR1-MAC mice for all of the drugs tested (Table 2).

Comparison of Transport Activity per P-gp Molecule of Seven P-gp Substrates between WT and hMDR1-MAC Mice. Since the results suggested that functional P-gp was expressed at the BBB of hMDR1-MAC mice, we finally examined the species differences of P-gp function between mice and humans by comparing transport activity per P-gp molecule of various P-gp substrates between WT and hMDR1-MAC mice. The values of transport activity per P-gp molecule were calculated from the amounts of P-gp in brain capillaries of WT and hMDR1-MAC mice shown in Table 1 and the $K_{p,brain}$ ratios of each drug shown in Table 2. Figure 5 shows the P-gp transport activity ratios of WT to hMDR1-MAC mice for the seven drugs. The ratios were ranged from 3.6-fold for loperamide to 0.85-fold for indinavir.

Discussion

We successfully generated a novel P-gp humanized mouse model using a MAC vector with chromosome-engineering techniques. A MAC vector has several advantages as a gene-delivery method compared with conventional plasmid and viral vectors (Oshimura et al., 2015; Satoh et al., 2018). One of the notable features of a MAC vector is maintained independently with a certain copy number in host cells. In addition, a MAC vector has no limitation on DNA size to be introduced and can carry the entire gene-containing regulatory region. These advantages of a MAC vector enable well-controlled and physiologic expression of a transgene in transgenic mice. In this study, hMDR1-MAC mice were generated using a MAC vector containing the entire *hMDR1* gene, whereas P-gp humanized mice were generated using a plasmid vector containing only protein-coding regions of the *hMDR1* gene in the previous study (Sadiq et al., 2015). Thus, the present study is the first success in which P-gp containing regulatory regions was humanized.

As expected, the expression of hMDR1 mRNA was detected in all of the examined tissues of hMDR1-MAC mice (Fig. 2). In addition, the expression of human P-gp was detected in brain capillaries of hMDR1-MAC mice but not in those of WT and Mdr1a/1b-KO mice (Table 1). Furthermore, the brain-to-plasma ratios of seven P-gp substrates were markedly lower in hMDR1-MAC mice than in Mdr1a/1b-KO mice (Fig. 3C; Table 2), and the brain-to-plasma ratio of paclitaxel was significantly increased by pretreatment with elacridar in hMDR1-MAC mice (Fig. 3F). These results clearly demonstrated that hMDR1-MAC mice express functional human P-gp in brain capillaries. Since previously reported P-gp humanized mice did not express functional P-gp at the BBB (Sadiq et al., 2015), the hMDR1-MAC mouse is the first P-gp humanized mouse model expressing functional P-gp in brain capillaries. Furthermore, the mice may be valuable for predicting P-gp–mediated drug-drug interactions at the BBB, although the effect of a P-gp inhibitor on the brain distribution of drugs is limited in a clinical setting (Sasongko et al., 2005; Hsiao et al., 2006; Muzi et al., 2009; Wagner et al., 2009; Bauer et al., 2015).

The results of this study showed that the amount of human P-gp in the isolated brain capillary fraction of hMDR1-MAC mice was smaller than the amount of mouse P-gp in that of WT mice (Table 1). This finding is consistent with the results of a previous study showing that the amount of P-gp in brain capillary fraction of humans was smaller than that in mice (Uchida et al., 2011b). The differences between hMDR1-MAC and WT mice in the expression level of P-gp in brain capillaries may mimic the differences between humans and mice. Mrp4 and Bcrp are ABC transporters expressed at the BBB, and Na^+,K^+-ATPase is a membrane protein selectively expressed at the plasma membrane. The expression levels of these proteins were 1.6-fold to 1.7-fold higher in hMDR1-MAC mice than those in WT mice (Table 1). Although the possibility of induction of these proteins by the introduction of MAC vector in hMDR1-MAC mice cannot be excluded, the difference in the expression levels of these proteins between WT and hMDR1-MAC mice is likely to be due to differences in the purity and homogeneity of brain capillaries in isolated fractions. Thus, the amount of P-gp in brain capillary fraction of hMDR1-MAC mice appears to be lower than that of WT even if the purity and homogeneity are comparable.

Measurement of the amount of P-gp by LC-MS/MS analysis was absolute quantification. Therefore, the amounts of the protein observed in hMDR1-MAC mice can be compared with those in humans. As shown in Table 1, the amount of P-gp in the isolated brain capillary fraction of hMDR1-MAC mice was 2.21 fmol/μg of protein (Table 1), whereas the amounts in humans were reported to be 6.06 and 3.98 fmol/μg of protein (Shawahna et al., 2011; Uchida et al., 2011b). Since the difference in purity and homogeneity of brain capillaries among the studies cannot be excluded, the expression of P-gp in brain capillaries appeared to be comparable at the order level in humans and hMDR1-MAC mice.

One of the major concerns is whether there are species differences in P-gp substrate susceptibility between humans and mice, because the results of previous studies regarding species differences in P-gp substrate susceptibility are controversial (Yamazaki et al., 2001; Takeuchi et al., 2006; Baltes et al., 2007; Feng et al., 2008; Chu et al., 2013). The present study showed differences in Kp,brain values of P-gp substrates between WT and hMDR1-MAC mice (Table 2), suggesting that the brain distributions of P-gp substrates are different in WT and hMDR1-MAC mice. We subsequently calculated the P-gp transport activity per

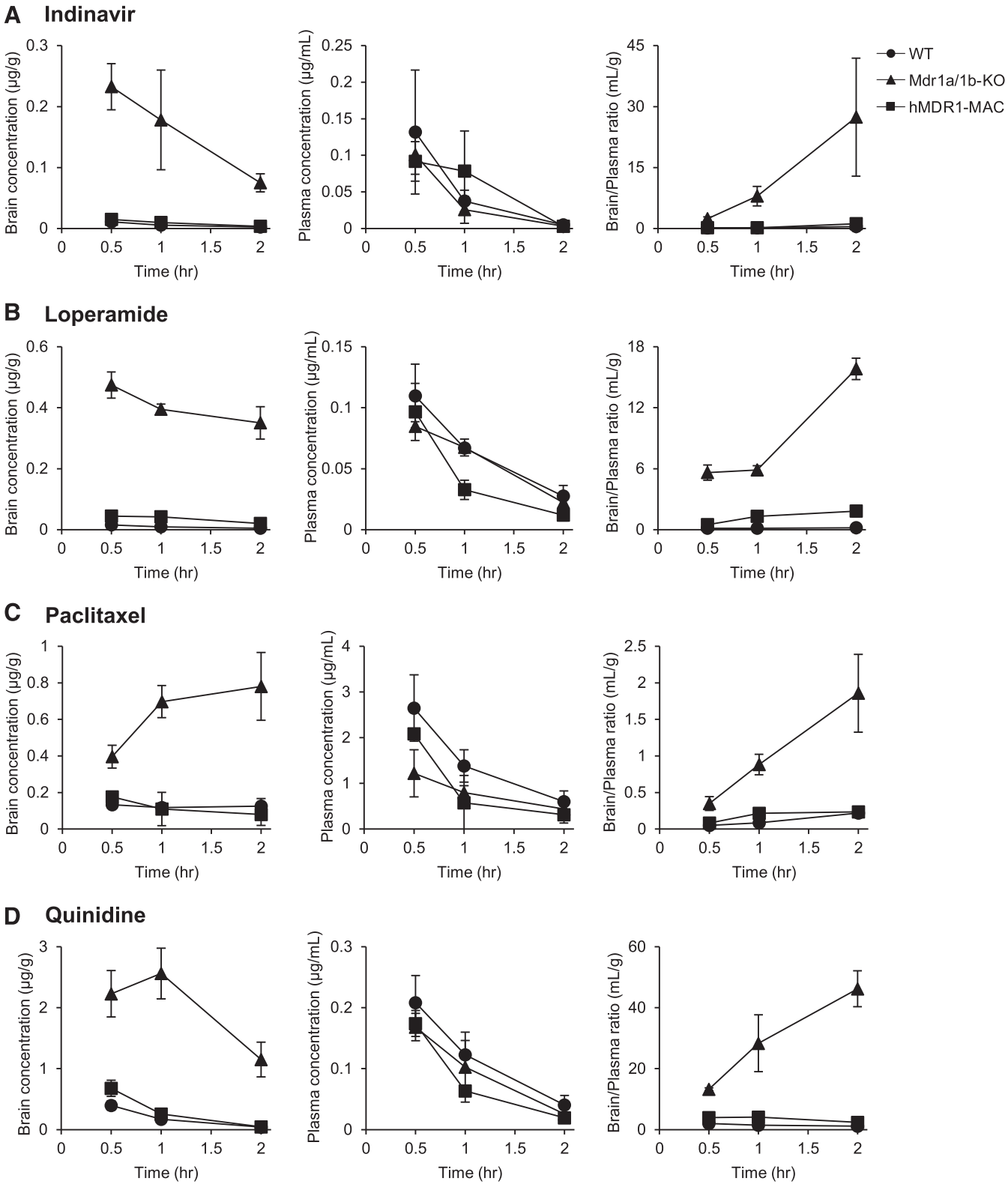

Fig. 4. Time profiles of brain and plasma concentrations and brain-to-plasma concentration ratios for seven P-gp substrates in WT, Mdr1a/1b-KO, and hMDR1-MAC mice. Mice (n = 3–6/time point) were intravenously administered indinavir sulfate (5 mg/kg) (A), loperamide hydrochloride (2 mg/kg) (B), paclitaxel (2 mg/kg) (C), quinidine sulfate (10 mg/kg) (D), ritonavir (5 mg/kg) (E), verapamil hydrochloride (1 mg/kg) (F), or vinblastine sulfate (4 mg/kg) (G) through the tail vein. Brains and plasma were collected at 0.5, 1, and 2 hours after the administration of each drug. Concentrations of drugs in brains and plasma were determined by LC-MS/MS, with each session performed in duplicate. Brain concentrations (left panels), plasma concentrations (middle panels), and brain-to-plasma ratios (right panels) of P-gp substrates. Data are shown as the mean ± S.D. of three to six mice.

molecule to evaluate the function of P-gp excluding the difference in the expression of P-gp at the BBB. This calculation is based on the hypothesis that the difference between WT and hMDR1-MAC mice simply exists in the expression and function of P-gp. If there is no difference in P-gp function between WT and hMDR1-MAC mice, the P-gp transport activity ratio of WT to hMDR1-MAC mice should be the

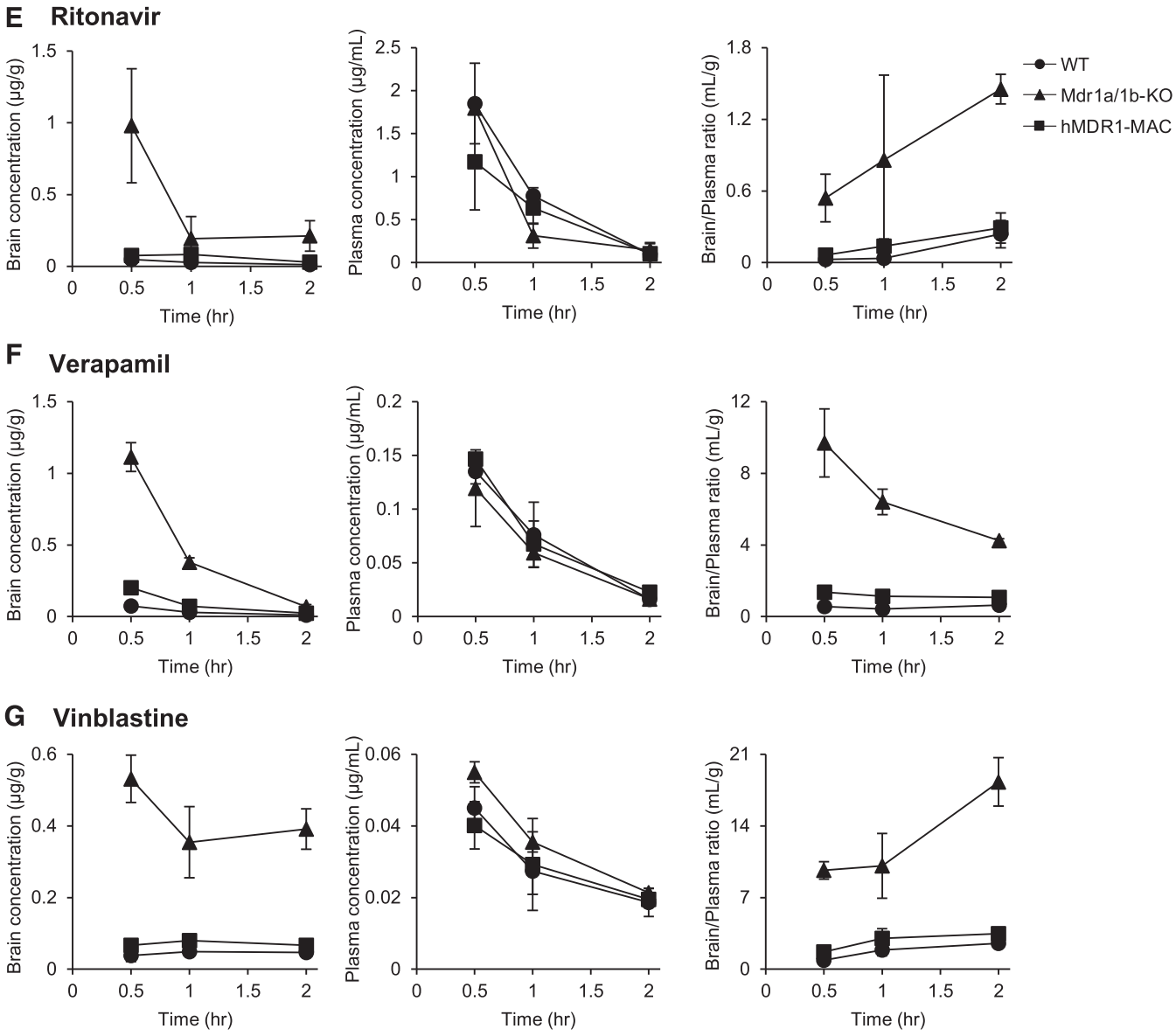

Fig. 4. continued.

same for the seven P-gp substrates. However, the P-gp transport activity ratios were different, ranging from 0.85 to 3.6 among the substrates (Fig. 5), suggesting that P-gp functions were different between WT and hMDR1-MAC mice. These results implied that there are species differences in P-gp substrate susceptibility between humans and mice. The hMDR1-MAC mice are expected to be a useful model for evaluation of the species differences of P-gp between humans and mice in vivo. The brain distribution of P-gp substrates is actually affected by many factors, including the expression and function of P-gp and other transporters, changes in P-gp expression caused by drugs, and the unbound fraction in plasma and the brain. To verify more explicitly the differences of P-gp observed in hMDR1-MAC and WT mice, it is necessary to consider the differences in factors other than the expression and function of P-gp examined in this study.

In addition to the brain, P-gp is expressed in various organs including the intestine, in which P-gp plays a key role in limiting the oral bioavailability of drugs (Ayrton and Morgan, 2001; Leslie et al., 2005; Callaghan et al., 2008; Hodges et al., 2011). Being consistent with previous studies (Sparreboom et al., 1997; Bardelmeijer et al., 2000), Mdr1a/1b-KO mice used in this study showed higher plasma levels of paclitaxel than WT mice (data not shown). On the other hand, hMDR1-MAC mice showed almost the same plasma levels of paclitaxel as Mdr1a/1b-KO mice (data not shown), suggesting that there was no limitation in the intestinal absorption of paclitaxel by P-gp in the intestine of hMDR1-MAC mice. This can be explained by the amount of P-gp in intestinal epithelial cells of hMDR1-MAC mice, which was extremely low compared with that in WT mice (Supplemental Table 5). These findings suggested that the expression levels of P-gp were insufficient to exert the function of P-gp in the intestine of hMDR1-MAC mice, although the reasons for the insufficient expression are still unclear. hMDR1-MAC encodes the upstream and downstream regions of the *hMDR1* gene (124 and 106 kb, respectively) in addition to the entire *hMDR1* gene (210 kb) including all exons and introns. Since the response elements of pregnane X receptor (PXR) are located approximately 8 kb upstream from the transcription start site of the *hMDR1* gene (Geick et al., 2001), PXR activators would regulate the gene expression of *hMDR1* in hMDR1-MAC mice. Our preliminary experiment showed that treatment with pregnenolone 16a-carbonitrile, a

TABLE 2

$AUC_{plasma\ (0–2\ hr)}$, $AUC_{brain\ (0–2\ hr)}$, $K_{p,brain}$ and $K_{p,brain}$ ratios of seven P-gp substrates in WT, Mdr1a/1b-KO and hMDR1-MAC mice

$AUC_{plasma\ (0–2\ hour)}$ and $AUC_{brain\ (0–2\ hour)}$ were calculated using the trapezoidal rule and are shown in ng/ml per hour and ng/g per hour, respectively. $K_{p,brain}$ is shown in milliliters per gram of the brain. $K_{p,brain}$ ratio was determined as ($K_{p,brain}$ in Mdr1a/1b-KO mice)/($K_{p,brain}$ in WT or hMDR1-MAC mice).

Substrate	WT	Mdr1a/1b-KO	hMDR1-MAC
Indinavir			
$AUC_{plasma\ (0–2\ hour)}$	188	141	224
$AUC_{brain\ (0–2\ hour)}$	10.6	287	16.4
$K_{p,brain}$	0.0562	2.03	0.0735
$K_{p,brain}$ ratio	36.2		27.7
Loperamide			
$AUC_{plasma\ (0–2\ hour)}$	162	141	119
$AUC_{brain\ (0–2\ hour)}$	17.2	708	64.0
$K_{p,brain}$	0.107	5.03	0.539
$K_{p,brain}$ ratio	47.2		9.33
Paclitaxel			
$AUC_{plasma\ (0–2\ hour)}$	3660	1840	2330
$AUC_{brain\ (0–2\ hour)}$	218	1110	210
$K_{p,brain}$	0.0594	0.603	0.0900
$K_{p,brain}$ ratio	10.2		6.70
Quinidine			
$AUC_{plasma\ (0–2\ hour)}$	307	258	223
$AUC_{brain\ (0–2\ hour)}$	346	3610	555
$K_{p,brain}$	1.13	14.0	2.49
$K_{p,brain}$ ratio	12.4		5.63
Ritonavir			
$AUC_{plasma\ (0–2\ hour)}$	2860	1860	1840
$AUC_{brain\ (0–2\ hour)}$	49.7	740	112
$K_{p,brain}$	0.0174	0.397	0.0608
$K_{p,brain}$ ratio	22.9		6.53
Verapamil			
$AUC_{plasma\ (0–2\ hour)}$	206	169	199
$AUC_{brain\ (0–2\ hour)}$	64.9	876	167
$K_{p,brain}$	0.315	5.17	0.838
$K_{p,brain}$ ratio	16.4		6.16
Vinblastine			
$AUC_{plasma\ (0–2\ hour)}$	66.0	82.5	64.0
$AUC_{brain\ (0–2\ hour)}$	79.2	727	126
$K_{p,brain}$	1.20	8.81	1.97
$K_{p,brain}$ ratio	7.34		4.47

typical ligand of murine PXR, tended to increase the expression level of hMDR1 mRNA in the intestine of hMDR1-MAC mice (data not shown), suggesting that PXR-mediated gene regulation of *hMDR1* is active even in the intestine of hMDR1-MAC mice. The expression of P-gp in the intestine of hMDR1-MAC mice may be affected by diet (Renaud et al., 2014) or unexpected systems such as species-specific microRNA (Yin et al., 2016). In any case, the improvement is necessary to increase the expression of P-gp in the intestine of hMDR1-MAC mice.

It is known that P-gp is also expressed in other tissues, including the liver, kidney, and testis, in which P-gp regulates biliary excretion, renal secretion, and testis distribution of drugs, respectively (Ayrton and Morgan, 2001; Leslie et al., 2005; Callaghan et al., 2008; Hodges et al., 2011; Mruk et al., 2011). As expected, hMDR1 mRNA was detected in various tissues other than the brain and intestine, including the liver, kidney, spleen, adrenal gland, testis, stomach, thymus, and heart, of hMDR1-MAC mice (Fig. 2). Further studies are needed to elucidate the expression and function of human P-gp in these tissues of hMDR1-MAC mice.

A number of single-nucleotide polymorphisms (SNPs) in the *hMDR1* gene have been identified. Many studies have been carried out to establish the role of *hMDR1* SNPs in various phenotypes such as P-gp expression, function, drug response, and disease susceptibility (Leschziner et al., 2007; Hodges et al., 2011; Fung et al., 2016). However, the reported effects of *hMDR1* SNPs are often inconclusive. Regarding the most common SNPs in the protein coding region

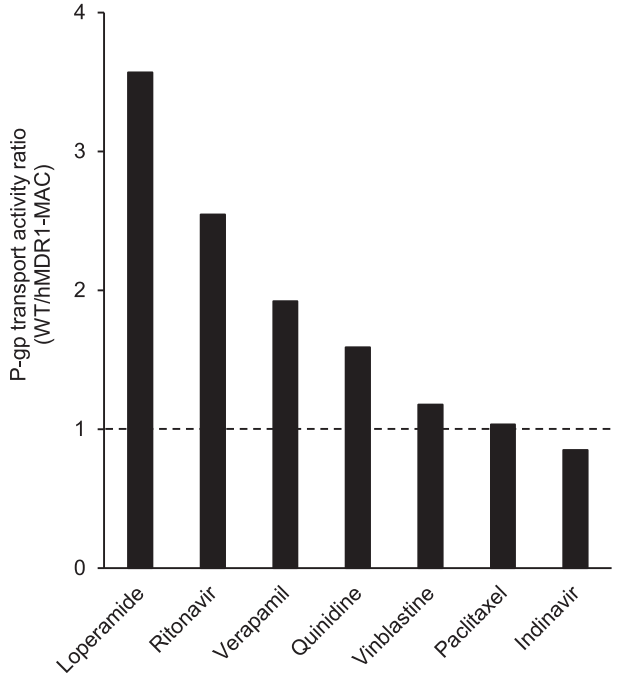

Fig. 5. P-gp transport activity ratios of WT to hMDR1-MAC mice for seven P-gp substrates. The transport activity per P-gp molecule was calculated as [($K_{p,brain}$ ratio) − 1]/[P-gp expression levels in brain capillaries of WT and hMDR1-MAC mice]. The data for P-gp expression levels and $K_{p,brain}$ ratio were taken from Tables 1 and 2.

[rs1128503 (1236T > C, Gly412Gly), rs2032582 (2677T > G/A, Ser893Ala/Thr), and rs1045642 (3435T > C, Ile1145Ile)], many pharmacokinetic and disease association studies focused on the role of these three SNPs, with controversial results. The sequences at the positions of these SNPs were all WT in the *hMDR1* gene embedded in the MAC vector in this study (data not shown). Recently, we generated CYP3A-humanized mice carrying SNPs in the *CYP3A5* gene and successfully reproduced the effects of SNPs on the expression of CYP3A5 (Abe et al., 2017; Uno et al., 2018). The development of hMDR1-MAC mice carrying the *hMDR1* SNPs may lead to clarification of the effects of SNPs on the expression and function of P-gp at the BBB.

Some studies have shown species differences of other transporters and drug-metabolizing enzymes between humans and mice (Martignoni et al., 2006; Chu et al., 2013). Hence, the applicability of a humanized animal model with humanization of only P-gp is probably limited for predicting pharmacokinetics of drugs in humans. The MAC vector can possibly overcome this limitation, since the MAC has no limitation on DNA size to be introduced and can carry multiple genes. If we are able to generate a mouse model in which several transporters and drug-metabolizing enzymes are humanized with the MAC, the pharmacokinetics of drugs in humans in vivo may be predicted more accurately by overcoming the problem of species differences in various transporters and enzymes. Further development of humanized mouse models utilizing the MAC and chromosome-engineering techniques is needed for more accurate prediction of the pharmacokinetics of drugs in humans in vivo.

In summary, a P-gp humanized mouse model was generated in this study. The results of the present study showed that hMDR1-MAC mice express functional human P-gp in brain capillaries and are effective for predicting the impact of human P-gp at the BBB on the brain distribution of drugs in vivo. On the other hand, the expression levels of P-gp were insufficient to exert the function of P-gp in the intestine of hMDR1-MAC mice. Improvement is needed to increase the expression of intestinal P-gp. The results also showed that hMDR1-MAC mice may reflect the expression and function of human P-gp at the BBB and are a

useful model for the evaluation of the species differences of P-gp between humans and mice in vivo. Therefore, this mouse line is a promising model for estimating the brain distribution of drugs in humans while taking into account species differences of P-gp.

Acknowledgments

We thank Toko Kurosaki, Yukako Sumida, Masami Morimura, Kei Yoshida, Eri Kaneda, Akiko Ashiba, Chie Ishihara, Kiyoko Kawakami, and Chiga Igawa at Tottori University, and Minori Osamura and Naoki Cho at Chiba University for technical assistance in the experiments. We also thank Dr. Hiroyuki Kugoh and Dr. Masaharu Hiratsuka at Tottori University for critical discussions.

Authorship Contributions

Participated in research design: Yamasaki, Kobayashi, Okuya, and Y. Kazuki.

Conducted experiments: Yamasaki, Okuya, Kajitani, K. Kazuki, Abe, Takehara, Ito, Ogata, Uemura, and Minegishi.

Performed data analysis: Yamasaki, Okuya, Ito, Ohtsuki, and Y. Kazuki.

Wrote or contributed to the writing of the manuscript: Yamasaki, Kobayashi, Ohtsuki, Akita, Chiba, Oshimura, and Y. Kazuki.

References

Abe S, Kobayashi K, Oji A, Sakuma T, Kazuki K, Takehara S, Nakamura K, Okada A, Tsukazaki Y, Senda N, et al. (2017) Modification of single-nucleotide polymorphism in a fully humanized CYP3A mouse by genome editing technology. *Sci Rep* **7**:15189.

Akazawa T, Uchida Y, Tachikawa M, Ohtsuki S, and Terasaki T (2016) Quantitative targeted absolute proteomics of transporters and pharmacoproteomics-based reconstruction of P-glycoprotein function in mouse small intestine. *Mol Pharm* **13**:2443–2456.

Ayrton A and Morgan P (2001) Role of transport proteins in drug absorption, distribution and excretion. *Xenobiotica* **31**:469–497.

Baltes S, Gastens AM, Fedrowitz M, Potschka H, Kaever V, and Löscher W (2007) Differences in the transport of the antiepileptic drugs phenytoin, levetiracetam and carbamazepine by human and mouse P-glycoprotein. *Neuropharmacology* **52**:333–346.

Bardelmeijer HA, Beijnen JH, Brouwer KR, Rosing H, Nooijen WJ, Schellens JH, and van Tellingen O (2000) Increased oral bioavailability of paclitaxel by GF120918 in mice through selective modulation of P-glycoprotein. *Clin Cancer Res* **6**:4416–4421.

Bauer M, Karch R, Zeitlinger M, Philippe C, Römermann K, Stanek J, Maier-Salamon A, Wadsak W, Jäger W, Hacker M, et al. (2015) Approaching complete inhibition of P-glycoprotein at the human blood-brain barrier: an (R)-[11C]verapamil PET study. *J Cereb Blood Flow Metab* **35**:743–746.

Callaghan R, Crowley E, Potter S, and Kerr ID (2008) P-glycoprotein: so many ways to turn it on. *J Clin Pharmacol* **48**:365–378.

Chen C, Hanson E, Watson JW, and Lee JS (2003) P-glycoprotein limits the brain penetration of nonsedating but not sedating H1-antagonists. *Drug Metab Dispos* **31**:312–318.

Chu X, Bleasby K, and Evers R (2013) Species differences in drug transporters and implications for translating preclinical findings to humans. *Expert Opin Drug Metab Toxicol* **9**:237–252.

Chu X, Zhang Z, Yabut J, Horwitz S, Levorse J, Li XQ, Zhu L, Lederman H, Ortiga R, Strauss J, et al. (2012) Characterization of multidrug resistance 1a/P-glycoprotein knockout rats generated by zinc finger nucleases. *Mol Pharmacol* **81**:220–227.

Dallas S, Salphati L, Gomez-Zepeda D, Wanek T, Chen L, Chu X, Kunta J, Mezler M, Menet MC, Chasseigneaux S, et al. (2016) Generation and characterization of a breast cancer resistance protein humanized mouse model. *Mol Pharmacol* **89**:492–504.

European Medicines Agency (2012) *Guideline on the Investigation of Drug Interactions, CPMP/EWP/560/95/Rev. 1 Corr. 2*, European Medicines Agency, London.

Feng B, Mills JB, Davidson RE, Mireles RJ, Janiszewski JS, Troutman MD, and de Morais SM (2008) In vitro P-glycoprotein assays to predict the in vivo interactions of P-glycoprotein with drugs in the central nervous system. *Drug Metab Dispos* **36**:268–275.

Food and Drug Administration (2017) *In Vitro Metabolism- and Transporter- Mediated Drug-Drug Interaction Studies Guidance for Industry, Draft Guidance*, Food and Drug Administration, Silver Spring, MD.

Fung KL, Hunt RC, Kimchi-Sarfaty C, and Gottesman MM (2016) Genetic polymorphisms of P-glycoprotein: echoes of silence, in *ABC Transporters-40 Years On* (George AM, ed) pp 105–134, Springer International Publishing AG, Basel, Switzerland.

Geick A, Eichelbaum M, and Burk O (2001) Nuclear receptor response elements mediate induction of intestinal MDR1 by rifampin. *J Biol Chem* **276**:14581–14587.

Giacomini KM, Huang SM, Tweedie DJ, Benet LZ, Brouwer KL, Chu X, Dahlin A, Evers R, Fischer V, Hillgren KM, et al.; International Transporter Consortium (2010) Membrane transporters in drug development. *Nat Rev Drug Discov* **9**:215–236.

Hodges LM, Markova SM, Chinn LW, Gow JM, Kroetz DL, Klein TE, and Altman RB (2011) Very important pharmacogene summary: ABCB1 (MDR1, P-glycoprotein). *Pharmacogenet Genomics* **21**:152–161.

Hsiao P, Sasongko L, Link JM, Mankoff DA, Muzi M, Collier AC, and Unadkat JD (2006) Verapamil P-glycoprotein transport across the rat blood-brain barrier: cyclosporine, a concentration inhibition analysis, and comparison with human data. *J Pharmacol Exp Ther* **317**:704–710.

Kazuki Y, Kobayashi K, Aueviriyavit S, Oshima T, Kuroiwa Y, Tsukazaki Y, Senda N, Kawakami H, Ohtsuki S, Abe S, et al. (2013) Trans-chromosomic mice containing a human CYP3A cluster for prediction of xenobiotic metabolism in humans. *Hum Mol Genet* **22**:578–592.

Leschziner GD, Andrew T, Pirmohamed M, and Johnson MR (2007) ABCB1 genotype and PGP expression, function and therapeutic drug response: a critical review and recommendations for future research. *Pharmacogenomics J* **7**:154–179.

Leslie EM, Deeley RG, and Cole SP (2005) Multidrug resistance proteins: role of P-glycoprotein, MRP1, MRP2, and BCRP (ABCG2) in tissue defense. *Toxicol Appl Pharmacol* **204**:216–237.

Martignoni M, Groothuis GM, and de Kanter R (2006) Species differences between mouse, rat, dog, monkey and human CYP-mediated drug metabolism, inhibition and induction. *Expert Opin Drug Metab Toxicol* **2**:875–894.

Masuda T, Tomita M, and Ishihama Y (2008) Phase transfer surfactant-aided trypsin digestion for membrane proteome analysis. *J Proteome Res* **7**:731–740.

Mruk DD, Su L, and Cheng CY (2011) Emerging role for drug transporters at the blood-testis barrier. *Trends Pharmacol Sci* **32**:99–106.

Muzi M, Mankoff DA, Link JM, Shoner S, Collier AC, Sasongko L, and Unadkat JD (2009) Imaging of cyclosporine inhibition of P-glycoprotein activity using 11C-verapamil in the brain: studies of healthy humans. *J Nucl Med* **50**:1267–1275.

Nakamura K, Hirayama-Kurogi M, Ito S, Kuno T, Yoneyama T, Obuchi W, Terasaki T, and Ohtsuki S (2016) Large-scale multiplex absolute protein quantification of drug-metabolizing enzymes and transporters in human intestine, liver, and kidney microsomes by SWATH-MS: comparison with MRM/SRM and HR-MRM/PRM. *Proteomics* **16**:2106–2117.

Oshimura M, Uno N, Kazuki Y, Katoh M, and Inoue T (2015) A pathway from chromosome transfer to engineering resulting in human and mouse artificial chromosomes for a variety of applications to bio-medical challenges. *Chromosome Res* **23**:111–133.

Renaud HJ, Cui JY, Lu H, and Klaassen CD (2014) Effect of diet on expression of genes involved in lipid metabolism, oxidative stress, and inflammation in mouse liver-insights into mechanisms of hepatic steatosis. *PLoS One* **9**:e88584.

Sadiq MW, Uchida Y, Hoshi Y, Tachikawa M, Terasaki T, and Hammarlund-Udenaes M (2015) Validation of a P-glycoprotein (P-gp) humanized mouse model by integrating selective absolute quantification of human MDR1, mouse Mdr1a and Mdr1b protein expressions with in vivo functional analysis for blood-brain barrier transport. *PLoS One* **10**:e0118638.

Sasongko L, Link JM, Muzi M, Mankoff DA, Yang X, Collier AC, Shoner SC, and Unadkat JD (2005) Imaging P-glycoprotein transport activity at the human blood-brain barrier with positron emission tomography. *Clin Pharmacol Ther* **77**:503–514.

Satoh D, Abe S, Kobayashi K, Nakajima Y, Oshimura M, and Kazuki Y (2018) Human and mouse artificial chromosome technologies for studies of pharmacokinetics and toxicokinetics. *Drug Metab Pharmacokinet* **33**:17–30.

Scheer N, Balimane P, Hayward MD, Buechel S, Kauselmann G, and Wolf CR (2012) Generation and characterization of a novel multidrug resistance protein 2 humanized mouse line. *Drug Metab Dispos* **40**:2212–2218.

Schinkel AH, Mayer U, Wagenaar E, Mol CA, van Deemter L, Smit JJ, van der Valk MA, Voordouw AC, Spits H, van Tellingen O, et al. (1997) Normal viability and altered pharmacokinetics in mice lacking mdr1-type (drug-transporting) P-glycoproteins. *Proc Natl Acad Sci USA* **94**:4028–4033.

Schinkel AH, Smit JJ, van Tellingen O, Beijnen JH, Wagenaar E, van Deemter L, Mol CA, van der Valk MA, Robanus-Maandag EC, te Riele HP, et al. (1994) Disruption of the mouse mdr1a P-glycoprotein gene leads to a deficiency in the blood-brain barrier and to increased sensitivity to drugs. *Cell* **77**:491–502.

Shawahna R, Uchida Y, Declèves X, Ohtsuki S, Yousif S, Dauchy S, Jacob A, Chassoux F, Daumas-Duport C, Couraud PO, et al. (2011) Transcriptomic and quantitative proteomic analysis of transporters and drug metabolizing enzymes in freshly isolated human brain microvessels. *Mol Pharm* **8**:1332–1341.

Silva R, Vilas-Boas V, Carmo H, Dinis-Oliveira RJ, Carvalho F, de Lourdes Bastos M, and Remião F (2015) Modulation of P-glycoprotein efflux pump: induction and activation as a therapeutic strategy. *Pharmacol Ther* **149**:1–123.

Sparreboom A, van Asperen J, Mayer U, Schinkel AH, Smit JW, Meijer DK, Borst P, Nooijen WJ, Beijnen JH, and van Tellingen O (1997) Limited oral bioavailability and active epithelial excretion of paclitaxel (Taxol) caused by P-glycoprotein in the intestine. *Proc Natl Acad Sci USA* **94**:2031–2035.

Takeuchi T, Yoshitomi S, Higuchi T, Ikemoto K, Niwa S, Ebihara T, Katoh M, Yokoi T, and Asahi S (2006) Establishment and characterization of the transformants stably-expressing MDR1 derived from various animal species in LLC-PK1. *Pharm Res* **23**:1460–1472.

Takiguchi M, Kazuki Y, Hiramatsu K, Abe S, Iida Y, Takehara S, Nishida T, Ohbayashi T, Wakayama T, and Oshimura M (2014) A novel and stable mouse artificial chromosome vector. *ACS Synth Biol* **3**:903–914.

Uchida Y, Ohtsuki S, Kamiie J, and Terasaki T (2011a) Blood-brain barrier (BBB) pharmacoproteomics: reconstruction of in vivo brain distribution of 11 P-glycoprotein substrates based on the BBB transporter protein concentration, in vitro intrinsic transport activity, and unbound fraction in plasma and brain in mice. *J Pharmacol Exp Ther* **339**:579–588.

Uchida Y, Ohtsuki S, Katsukura Y, Ikeda C, Suzuki T, Kamiie J, and Terasaki T (2011b) Quantitative targeted absolute proteomics of human blood-brain barrier transporters and receptors. *J Neurochem* **117**:333–345.

Uchida Y, Tachikawa M, Obuchi W, Hoshi Y, Tomioka Y, Ohtsuki S, and Terasaki T (2013) A study protocol for quantitative targeted absolute proteomics (QTAP) by LC-MS/MS: application for inter-strain differences in protein expression levels of transporters, receptors, claudin-5, and marker proteins at the blood-brain barrier in ddY, FVB, and C57BL/6J mice. *Fluids Barriers CNS* **10**:21.

Uchida Y, Wakayama K, Ohtsuki S, Chiba M, Ohe T, Ishii Y, and Terasaki T (2014) Blood-brain barrier pharmacoproteomics-based reconstruction of the in vivo brain distribution of P-glycoprotein substrates in cynomolgus monkeys. *J Pharmacol Exp Ther* **350**:578–588.

Uno N, Abe S, Oshimura M, and Kazuki Y (2018) Combinations of chromosome transfer and genome editing for the development of cell/animal models of human disease and humanized animal models. *J Hum Genet* **63**:145–156.

Wagner CC, Bauer M, Karch R, Feurstein T, Kopp S, Chiba P, Kletter K, Löscher W, Müller M, Zeitlinger M, et al. (2009) A pilot study to assess the efficacy of tariquidar to inhibit P-glycoprotein at the human blood-brain barrier with (R)-11C-verapamil and PET. *J Nucl Med* **50**:1954–1961.

Yamazaki M, Neway WE, Ohe T, Chen I, Rowe JF, Hochman JH, Chiba M, and Lin JH (2001) In vitro substrate identification studies for p-glycoprotein-mediated transport: species difference and predictability of in vivo results. *J Pharmacol Exp Ther* **296**:723–735.

Yin S, Fan Y, Zhang H, Zhao Z, Hao Y, Li J, Sun C, Yang J, Yang Z, Yang X, et al. (2016) Differential TGFβ pathway targeting by miR-122 in humans and mice affects liver cancer metastasis. *Nat Commun* **7**:11012.

Address correspondence to: Dr. Yasuhiro Kazuki, Tottori University, 86 Nishi-cho, Yonago, Tottori 683-8503, Japan. E-mail: kazuki@grape.med.tottori-u.ac.jp and Dr. Kaoru Kobayashi, Chiba University, 1-8-1 Inohana, Chuo-ku, Chiba 260-8675, Japan. E-mail: kaoruk@faculty.chiba-u.jp

Title

Characterization of P-glycoprotein Humanized Mice Generated by Chromosome Engineering Technology: Its Utility for Prediction of Drug Distribution to the Brain in Humans

Names of Authors

Yuki Yamasaki, Kaoru Kobayashi, Fuka Okuya, Naoyo Kajitani, Kanako Kazuki, Satoshi Abe, Shoko Takehara, Shingo Ito, Seiryo Ogata, Tatsuki Uemura, Sumio Ohtsuki, Genki Minegishi, Hidetaka Akita, Kan Chiba, Mitsuo Oshimura, Yasuhiro Kazuki

Journal Title

Drug Metabolism and Disposition

Supplemental Materials and Methods

Sample preparation for paclitaxel

For the plasma and brains collected at 4 hr after the administration of paclitaxel, the preparation of samples was performed by the liquid-liquid extraction method in glass vials. Twenty μL of plasma or brain homogenate, 80 μL of blank pig serum, 20 μL of internal standard working solution and 1 mL of t-butyl methyl ether were added to the vials. The specimens were mixed by shaking for 10 min and centrifugated at 1,710 *g* for 10 min. Subsequently, the upper layer (organic layer) was transferred into a new glass vial and evaporated. The remaining residues were reconstituted with 200 μL of 60% methanol and then injected into the LC-MS/MS system.

For the plasma and brains collected at 0.5, 1 and 2 hr after the administration of paclitaxel, the preparation of samples was performed by the deproteinization method in polypropylene tubes. Twenty μL of internal standard working solution was added to tubes and evaporated. Subsequently, 20 μL of plasma or brain homogenate was added to the tubes. The proteins in theses samples were precipitated with 200 μL of acetonitrile. Then the specimens were mixed by vortex and centrifugated at 20,400 *g* for 10 min. The supernatant (180 μL) was diluted with 60 μL of water and then injected into the LC-MS/MS system.

Sample preparation for hydroxyzine

Twenty μL of internal standard working solution was added to polypropylene tubes and evaporated. Subsequently, 20 μL of plasma or brain homogenate was added to the tubes. The proteins in theses samples were precipitated with 200 μL of acetonitrile containing 0.1% formic acid. Then the specimens were mixed by vortex and centrifugated at 20,400 *g* for 10 min. The supernatant (160 μL) was diluted with 40 μL of water containing 0.1% formic acid and then injected into the LC-MS/MS system.

Sample preparation for indinavir and loperamide

Twenty μL of internal standard working solution was added to polypropylene tubes and

evaporated. Subsequently, 20 μL of plasma or brain homogenate was added to the tubes. The proteins in theses samples were precipitated with 200 μL of acetonitrile containing 0.1% formic acid. Then the specimens were mixed by vortex and centrifugated at 20,400 *g* for 10 min. The supernatant (180 μL) was diluted with 60 μL of water and then injected into the LC-MS/MS system.

Sample preparation for quinidine

Twenty μL of plasma or brain homogenate was added to polypropylene tubes. The proteins in theses samples were precipitated with 200 μL of a mixture of 0.1% formic acid in water-0.1% formic acid in acetonitrile (1:2, v/v) containing an internal standard. Then the specimens were mixed by vortex and centrifugated at 20,400 *g* for 10 min. The supernatant was injected into the LC-MS/MS system.

Sample preparation for ritonavir and vinblastine

Twenty μL of plasma or brain homogenate was added to polypropylene tubes. The proteins in theses samples were precipitated with 200 μL of a mixture of 0.1% formic acid in water with 5 mM ammonium acetate-0.1% formic acid in acetonitrile (1:2, v/v) containing an internal standard. Then the specimens were mixed by vortex and centrifugated at 20,400 *g* for 10 min. The supernatant was injected into the LC-MS/MS system.

Sample preparation for verapamil

Twenty μL of internal standard working solution was added to polypropylene tubes and evaporated. Subsequently, 20 μL of plasma or brain homogenate was added to the tubes. The proteins in theses samples were precipitated with 200 μL of acetonitrile containing 0.1% formic acid. Then the specimens were mixed by vortex and centrifugated at 20,400 *g* for 10 min. The supernatant (150 μL) was diluted with 50 μL of water containing 0.1% formic acid and then injected into the LC-MS/MS system.

LC-MS/MS analysis

The LC-MS/MS assay for quinidine, ritonavir and vinblastine was conducted using a Shimadzu LC-20AD Prominence HPLC pump (Shimadzu, Kyoto, Japan), a Shimadzu SIL-20AC HT

autosampler (Shimadzu), and an AB SCIEX QTRAP 4500 mass spectrometer (SCIEX). The LC-MS/MS assay for other compounds was conducted using a Hitachi LaChrom ULTRA L-2160U UPLC pump (Hitachi, Tokyo, Japan), a Hitachi LaChrom Elite L-2200 autosampler (Hitachi), and a Bruker amaZon SL mass spectrometer (Bruker Daltonics K.K., Billerica, MA). Samples were injected onto columns shown in Supplemental Table 4. The compounds were separated and eluted from the column under linear gradient conditions. The eluted compounds were detected by electrospray ionization using MRM mode.

Supplemental Table 1. Primers for genomic PCR analyses.

Primer sets used were as follows: hMDR1-1L/hMDR1-1R, hMDR1-2L/hMDR1-2R, hMDR1-3L/hMDR1-3R, hMDR1-4L/hMDR1-4R, hMDR1-5L/hMDR1-5R, hMDR1-6L/hMDR1-6R, hMDR1-7L/hMDR1-7R, hMDR1-8L/hMDR1-8R, and hMDR1-9L/hMDR1-9R for detection of the human MDR1 cluster; m11 4L/V907-NotI-R and hyg F(244)/m11 6R for detection of MAC4; MDR1loxP2L/BsdR and hprt332F/MDR1loxP1R for detection the targeting of pAC005045-loxP-BS at the pAC005045 locus; CYP3A4-4L/CYP3A4-3R and MDR1tel5L/SK23 for detection the chromosome truncation at the AC003083 locus; TRANS L1/TRANS R1 for detection the Cre-loxP-mediated chromosomal translocation between MAC and modified hChr.7; mMdr1a i6e7 L/R, mMdr1a int5 L/R, mMdr1b i3e4 L/R, mMdr1b e4i4 L/R, mMdr1ako i5hyg L/R, mMdr1ako hygi7 L/R and mMdr1ako neoi4 L/R for genotyping of mouse Mdr1a/b-KO.

Primer	**Sequence (5' to 3')**
hMDR1-1L	CTCCTAGGAGTACTCACTTC
hMDR1-1R	AACAGAAACATGGCTTGGCG
hMDR1-2L	CGCCAAGCCATGTTTCTGTTT
hMDR1-2R	AAGGAAATGCTTTCTGCCTTG
hMDR1-3L	GTGCAACGGAAGCCAGAACA
hMDR1-3R	AGCGGCCTCTGCTTCTTTGA
hMDR1-4L	CTGATTGGCTGGGCAGGAAC
hMDR1-4R	CTTGGAACGGCCACCAAGAC
hMDR1-5L	GGTGCTGGTTGCTGCTTACA
hMDR1-5R	CCCAACATCGTGCACATCAA
hMDR1-6L	GTCAGTGTTGATGGACAGGA
hMDR1-6R	GCATTGGCTTCCTTGACAGC

hMDR1-7L	GGTTCCAGGCTTGCTGTAAT
hMDR1-7R	TCTTTCAGTGCTTGTCCAGA
hMDR1-8L	GGCAAAGAAATAAAGCGACTG
hMDR1-8R	CCTCCTTTGCTGCCCTCACA
hMDR1-9L	TCTTGTCCAAACTGCCTGTGA
hMDR1-9R	TGCAAGAATCAGCAGGATCAA
m11 4L	ACTCCTAAGGGAGTTGGTGCTGTTGGTG
V907-NotI-R	AGATCTCGGCTAGAGGTACCCTAGAAGATC
hyg F(244)	GAATTCAGCGAGAGCCTGAC
m11 6R	CCCAGGAATCAGTCAGGAAGGCTGTAA
hMDR1loxP2L	GCCAAGTGTAGCTGGAGAATGATTCGTG
hMDR1loxP1R	ACAAGGCACTTCAGGATACCAAGCTTCC
BsdR	GCTCAAGATGCCCCTGTTCT
hprt332F	AAAGATGGTCAAGGTCGCAA
hMDR1tel5L	CTATTCTAAAAAGCTGCCTTGGCCCACA
hMDR1tel5R	TGTAGCCCAGTTCCTAATGGGACACAGA
SK23	GGCCGCTCTAGAACTAGTGGATC
CYP3A4-4L	TCCCCCTGAAATTAAGCTTA
CYP3A4-3R	TGAGGTCTCTGGTGTTCTCA
TRANS L1	TGGAGGCCATAAACAAGAAGAC
TRANS R1	CCCCTTGACCCAGAAATTCCA
mMdr1a i6e7 L	CCCCACAGTCCCAAAGAACT
mMdr1a i6e7 R	CCATTGCCTGGAAGAACATT
mMdr1a int5 L	CCCTGGCCTGAATGTATTTC

mMdr1a int5 R	TCTGGGTATTCCCCATCCTT
mMdr1b i3e4 L	GAACACAGCAGAGGGAGAGC
mMdr1b i3e4 R	TTTCCAAACACCAGCATCAA
mMdr1b e4i4 L	GCCAGTATTCTGCCAAGCAT
mMdr1b e4i4 R	ATAGCCATGGACGCTCAAAC
Mdr1ako i5hyg L	ATGGGACTTCCTTTGAACTCTTTCTTG
Mdr1ako i5hyg R	TTTCCACTATCGGCGAGTACTTCTACA
Mdr1ako hygi7 L	TCAATACACTACATGGCGTGATTTCAT
Mdr1ako hygi7 R	TCACATATTAGTGGTTGTGGTGGTTTG
Mdr1bko neoi4 L	GTGGAGAGGCTATTCGGCTATGACT
Mdr1bko neoi4 R	CACAGGTTTCTCCACTCTTCTGATGTT

Supplemental Table 2. PCR cycle numbers for RT-PCR.

Tissue	hMDR1	Mouse GAPDH
Brain	40	28
Intestine	38	30
Liver	38	30
Kidney	40	28
Spleen	40	30
Adrenal gland	36	30
Testis	38	28
Stomach	40	28
Thymus	40	28
Heart	40	26

Supplemental Table 3. MRM transitions used for multiplexed MRM analysis for determination of protein expression levels.

Protein	Amino acid sequence	Unlabeled peptide (m/z)					Labeled peptide (m/z)				
		Q1	Q3-1	Q3-2	Q3-3	Q3-4	Q1	Q3-1	Q3-2	Q3-3	Q3-4
hMDR1 and mdr1a	NTTGALTTR	467.8	377.2	490.3	618.4	719.4	471.3	377.2	497.3	625.4	726.4
Mdr1a	ATVSASHIIR	352.2	173.1	348.7	392.2	441.8	354.5	173.1	352.2	395.7	445.3
hMDR1	FYDPLAGK	455.7	275.2	311.1	485.3	600.3	457.7	279.2	311.1	489.3	604.3
Mdr1b	EAVDEDVPLVSFWR	831.4	659.3	904.5	1003.6	1118.6	836.4	659.3	758.3	914.5	1128.6
Mrp4	APVLFFDR	482.8	268.2	584.3	697.4	796.4	486.3	268.2	584.3	704.4	803.5
Bcrp	SSLLDVLAAR	522.8	430.3	529.3	644.4	757.5	526.3	437.3	536.4	651.4	764.5
Villin-1	YNDEPVQIR	567.3	393.1	612.4	741.4	856.5	572.3	393.1	622.4	751.4	866.5
Na^+, K^+- ATPase	VDNSSLTGESEPQTR	810.4	717.3	903.4	903.4	1004.5	813.4	723.4	909.4	1010.5	1123.6

Supplemental Table 4. Conditions used for LC-MS/MS analysis of compounds.

The column consisted of either a COSMOSIL 5C_{18}-MS-II Packed Column 2.0 × 150 mm, 5 µm (Column 1), a TSKgel ODS-100Z 2.0 × 150 mm, 5.0 µm (Column 2), or a COSMOSIL 3C_{18}-MS-II Packed Column 2.0 × 50 mm, 3 µm (Column 3). Mobile phases consisted of 0.1% formic acid in water (Mobile phase 1), 0.1% formic acid in water with 5 mM ammonium acetate (Mobile phase 2), 0.1% formic acid in acetonitrile (Mobile phase 3), and methanol (Mobile phase 4).

Standard		**Internal standard**		**Column**		**Flow rate**	**Injection volume**	**Mobile phases**		**Gradient condition**
Compound	**MRM transition**	**Compound**	**MRM transition**	**No.**	**Temp.**	**(mL/min)**	**(µL)**	**A (No.)**	**B (No.)**	**Time (min); B concentration %**
Hydroxyzine	m/z 375.2 → 200.9	Metoprolol	m/z 268.0 → 116.0	1	30°C	0.25	10	1	3	0-2 min; 5% → 6-14.5 min; 95% → 15 min; 5%
Indinavir	m/z 614.3 → 465.3	Verapamil	m/z 455.2 → 164.9	2	30°C	0.20	10	2	3	0-2 min; 10% → 7 min; 95% → 11.1-15 min; 10%
Loperamide	m/z 477.2 → 266.0	Haloperidol	m/z 376.1 → 164.9	2	30°C	0.20	10	1	3	0-2 min; 15% → 7 min; 95% → 11.1-15 min; 15%
Paclitaxel	m/z 876.4 → 308.0	Docetaxel	m/z 830.4 → 549.2	2	30°C	0.20	20 or 30	1	4	0-2 min; 70% → 9 min; 90% → 11.6-15 min; 70%
Quinidine	m/z 325.2 → 160.1	Verapamil	m/z 455.2 → 165.1	3	40°C	0.60	3	1	3	0-1.2 min; 5% → 2 min; 90% → 3.71-5 min; 5%
Ritonavir	m/z 721.3 → 268.1	Indinavir	m/z 614.4 → 465.2	3	40°C	0.60	3	2	3	0-1 min; 20% → 1.9 min; 90% → 3.41-4.7 min; 20%
Verapamil	m/z 455.2 → 164.9	Indinavir	m/z 614.3 → 465.3	2	30°C	0.30	10	1	3	0-2 min; 15% → 6 min; 95% → 8.01-9 min; 15%
Vinblastine	m/z 406.3 → 376.2	Verapamil	m/z 455.2 → 165.1	3	40°C	0.60	5	2	3	0-0.5 min; 15% → 2 min; 90% → 3.71-5 min; 15%

Supplemental Table 5. Protein expression levels of membrane proteins in the plasma membrane fraction of intestinal epithelial cells isolated from WT, Mdr1a/1b-KO and hMDR1-MAC mice.

The plasma membrane fractions of intestinal epithelial cells were isolated from pooled small intestines of WT, Mdr1a/1b-KO and hMDR1-MAC mice (5 mice/group), and the protein expression levels were quantified by LC-MS/MS. The protein expression levels in four sets of transitions in three biological replicates were used to calculate the average (mean) and variability (S.E.M.), which are shown as mean ± S.E.M. ULQ, under the limit of quantification; peak area ratio was lower than the lowest point of the standard curve (0.5 fmol/5 μg protein). $^{**}p < 0.01$, significantly different from the protein expression amounts in the plasma membrane fraction of intestinal epithelial cells isolated from WT mice.

Molecular names	**Protein expression level (fmol/μg protein)**		
	WT	**Mdr1a/1b-KO**	**hMDR1-MAC**
Human MDR1 & Mouse Mdr1a [a]	4.57 ± 0.14	ULQ (< 0.10)	0.13 ± 0.02 [d] **
Human MDR1 [b]	ULQ (< 0.10)	ULQ (< 0.10)	0.17 ± 0.02 [d]
Mouse Mdr1a [c]	2.95 ± 0.06	ULQ (< 0.10)	ULQ (< 0.10)
Mouse Mdr1b	ULQ (< 0.10)	ULQ (< 0.10)	ULQ (< 0.10)
Mrp4	0.11 ± 0.00	0.11 ± 0.00	0.11 ± 0.01
Bcrp	7.37 ± 0.18	7.79 ± 0.18	7.13 ± 0.43
Villin-1	18.29 ± 0.34	12.52 ± 0.19**	20.47 ± 0.40**
Na^+, K^+-ATPase	264.16 ± 12.14	210.85 ± 9.14**	245.93 ± 10.60

[a] measured by using a peptide probe set common for human MDR1 and mouse Mdr1a.

[b] measured by using a peptide probe set specific for human MDR1.

[c] measured by using a peptide probe set specific for mouse Mdr1a.

[d] the value was determined from 2-3 transitions, and the reliability was lower than that of other values.

Supplemental Table 6. Time profiles of brain and plasma concentrations and brain-to-plasma concentration ratios for seven P-gp substrates in WT, Mdr1a/1b-KO and hMDR1-MAC mice.

Mice (n=3-6/time point) were intravenously administered indinavir sulfate (5 mg/kg), loperamide hydrochloride (2 mg/kg), 10 mg/kg paclitaxel (2 mg/kg), quinidine sulfate (10 mg/kg), ritonavir (5 mg/kg), verapamil hydrochloride (1 mg/kg) or vinblastine sulfate (4 mg/kg) through the tail vein. Brains and plasma were collected at 0.5, 1 and 2 hr after the administration of each drug. Concentrations of drugs in the brains and plasma were determined by LC-MS/MS, each performed in duplicate. Brain concentrations (ng/g), plasma concentrations (ng/mL) and brain-to-plasma ratios (mL/g) are shown as means ± S.D. of three-six mice. * $p < 0.05$ and ** $p < 0.01$ compared with Mdr1a/1b-KO mice.

Substrate	WT	Mdr1a/1b-KO	hMDR1-MAC
Indinavir			
0.5 hr			
Brain	10.9 ± 5.1**	233 ± 38	14.6 ± 0.9**
Plasma	132 ± 85	101 ± 27	91.7 ± 26.9
Brain-to-plasma ratio	0.0904 ± 0.0283**	2.37 ± 0.51	0.169 ± 0.052**
1 hr			
Brain	5.45 ± 1.71*	178 ± 82	9.86 ± 4.44*
Plasma	37.5 ± 14.7	25.6 ± 18.4	78.2 ± 55.0
Brain-to-plasma ratio	0.158 ± 0.060**	7.94 ± 2.38	0.182 ± 0.120**
2 hr			
Brain	2.14 ± 1.17**	74.9 ± 15.0	3.50 ± 1.66**
Plasma	4.82 ± 2.08	3.32 ± 1.65	2.96 ± 0.60
Brain-to-plasma ratio	0.449 ± 0.154*	27.4 ± 14.5	1.15 ± 0.33*

Loperamide

0.5 hr			
Brain	15.5 ± 0.9**	474 ± 43	44.6 ± 2.3**
Plasma	110 ± 26	84.7 ± 3.9	96.5 ± 23.5
Brain-to-plasma ratio	0.147 ± 0.039**	5.62 ± 0.75	0.479 ± 0.107**
1 hr			
Brain	9.42 ± 2.34**	395 ± 18	42.0 ± 6.0**
Plasma	66.9 ± 1.3	67.4 ± 7.0	32.7 ± 7.9**
Brain-to-plasma ratio	0.141 ± 0.034**	5.88 ± 0.41	1.31 ± 0.20**
2 hr			
Brain	4.85 ± 1.44**	350 ± 53	20.3 ± 2.9**
Plasma	27.5 ± 8.7	22.3 ± 4.7	11.9 ± 4.8
Brain-to-plasma ratio	0.179 ± 0.027**	15.8 ± 1.1	1.83 ± 0.55**

Paclitaxel

0.5 hr			
Brain	134 ± 20**	396 ± 63	176 ± 15**
Plasma	2650 ± 730*	1220 ± 510	2080 ± 100
Brain-to-plasma ratio	0.0518 ± 0.0080**	0.349 ± 0.094	0.0843 ± 0.0053**
1 hr			
Brain	118 ± 25**	697 ± 88	109 ± 91**
Plasma	1380 ± 350	800 ± 152	576 ± 598
Brain-to-plasma ratio	0.0858 ± 0.0041**	0.884 ± 0.139	0.215 ± 0.060**

2 hr			
Brain	125 ± 42**	780 ± 186	80.1 ± 60.5**
Plasma	600 ± 235	441 ± 138	316 ± 184
Brain-to-plasma ratio	0.219 ± 0.059**	1.86 ± 0.53	0.237 ± 0.044**
Quinidine			
0.5 hr			
Brain	395 ± 75**	2230 ± 380	678 ± 133**
Plasma	208 ± 44	168 ± 22	174 ± 21
Brain-to-plasma ratio	1.97 ± 0.62**	13.2 ± 0.5	3.95 ± 1.00**
1 hr			
Brain	170 ± 16**	2560 ± 420	258 ± 26**
Plasma	123 ± 23	103 ± 57	63.4 ± 7.3
Brain-to-plasma ratio	1.44 ± 0.44**	28.3 ± 9.3	4.08 ± 0.34**
2 hr			
Brain	42.6 ± 6.9**	1150 ± 280	44.6 ± 0.7**
Plasma	40.3 ± 15.8	25.6 ± 9.4	19.3 ± 4.6
Brain-to-plasma ratio	1.12 ± 0.25**	46.2 ± 5.9	2.42 ± 0.69**
Ritonavir			
0.5 hr			
Brain	47.6 ± 8.4**	980 ± 397	73.9 ± 43.8**
Plasma	1850 ± 470	1800 ± 80	1170 ± 560
Brain-to-plasma ratio	0.0264 ± 0.0054**	0.541 ± 0.200	0.0626 ± 0.0287**

1 hr			
Brain	26.8 ± 1.9	192 ± 154	81.3 ± 15.3
Plasma	777 ± 92**	313 ± 145	636 ± 187*
Brain-to-plasma ratio	0.0351 ± 0.0069	0.858 ± 0.713	0.139 ± 0.059
2 hr			
Brain	11.5 ± 2.9**	212 ± 106	27.8 ± 15.6**
Plasma	97.7 ± 135.0	147 ± 74	104 ± 66
Brain-to-plasma ratio	0.239 ± 0.114**	1.45 ± 0.12	0.290 ± 0.127**

Verapamil

0.5 hr			
Brain	74.6 ± 11.5**	1110 ± 100	201 ± 15**
Plasma	135 ± 12	119 ± 36	147 ± 2
Brain-to-plasma ratio	0.559 ± 0.128**	9.70 ± 1.91	1.37 ± 0.12**
1 hr			
Brain	30.0 ± 4.1**	380 ± 31	72.2 ± 5.5**
Plasma	76.0 ± 30.4	59.4 ± 2.2	67.7 ± 21.4
Brain-to-plasma ratio	0.421 ± 0.104**	6.41 ± 0.71	1.13 ± 0.30**
2 hr			
Brain	10.2 ± 1.34**	68.5 ± 16.3	24.1 ± 7.4**
Plasma	16.1 ± 2.8	16.2 ± 4.2	22.7 ± 5.8
Brain-to-plasma ratio	0.639 ± 0.030**	4.23 ± 0.11	1.07 ± 0.20**

Vinblastine

0.5 hr			
Brain	38.2 ± 17.4**	531 ± 66	66.4 ± 6.6**
Plasma	45.0 ± 6.0	55.0 ± 3.0	40.2 ± 6.6*
Brain-to-plasma ratio	0.879 ± 0.482**	9.65 ± 0.85	1.68 ± 0.32**
1 hr			
Brain	48.9 ± 4.4**	354 ± 99	79.5 ± 5.7**
Plasma	27.4 ± 6.5	35.5 ± 2.8	29.2 ± 12.9
Brain-to-plasma ratio	1.87 ± 0.56**	10.1 ± 3.2	3.00 ± 0.95*
2 hr			
Brain	46.9 ± 8.3**	391 ± 56	67.0 ± 7.4**
Plasma	18.7 ± 4.0	21.4 ± 1.1	19.5 ± 1.7
Brain-to-plasma ratio	2.53 ± 0.21**	18.3 ± 2.4	3.47 ± 0.58**

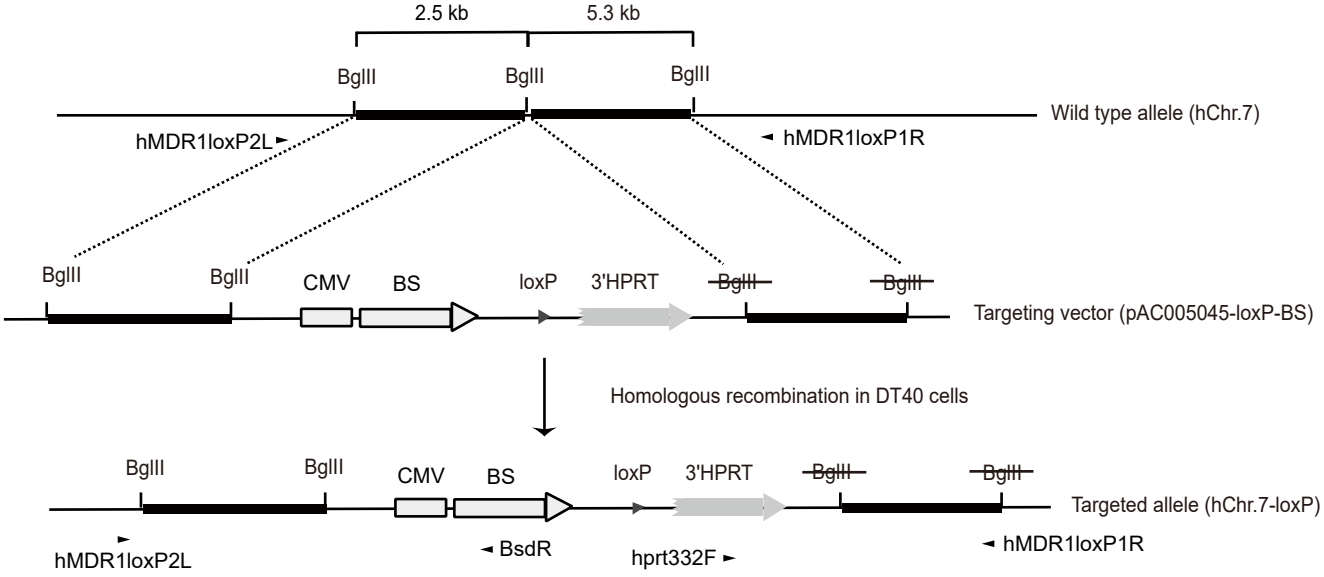

Supplemental Fig. 1. Targeted insertion of loxP at AC005045 locus on hChr.7. The wild-type locus of AC005045, pAC005045-loxP-BS targeting construct, and the targeted allele are shown.

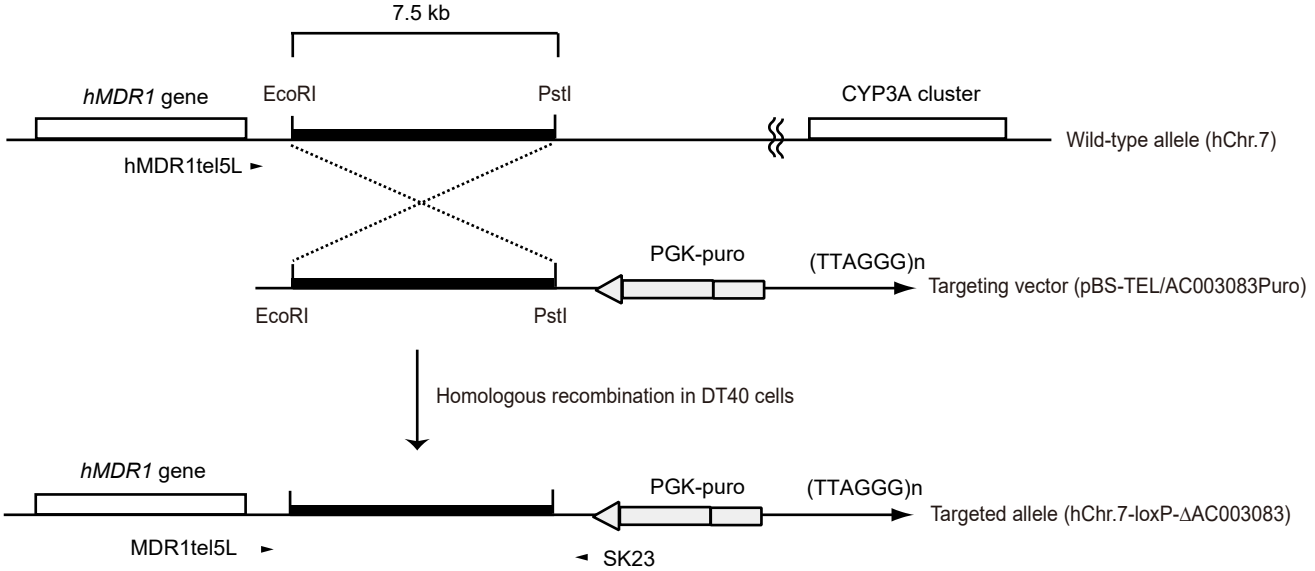

Supplemental Fig. 2. Targeted truncation at AC003083 on hChr.7. The wild-type locus of AC003083, pBS-TEL/AC003083Puro targeting construct, and the targeted allele are shown.

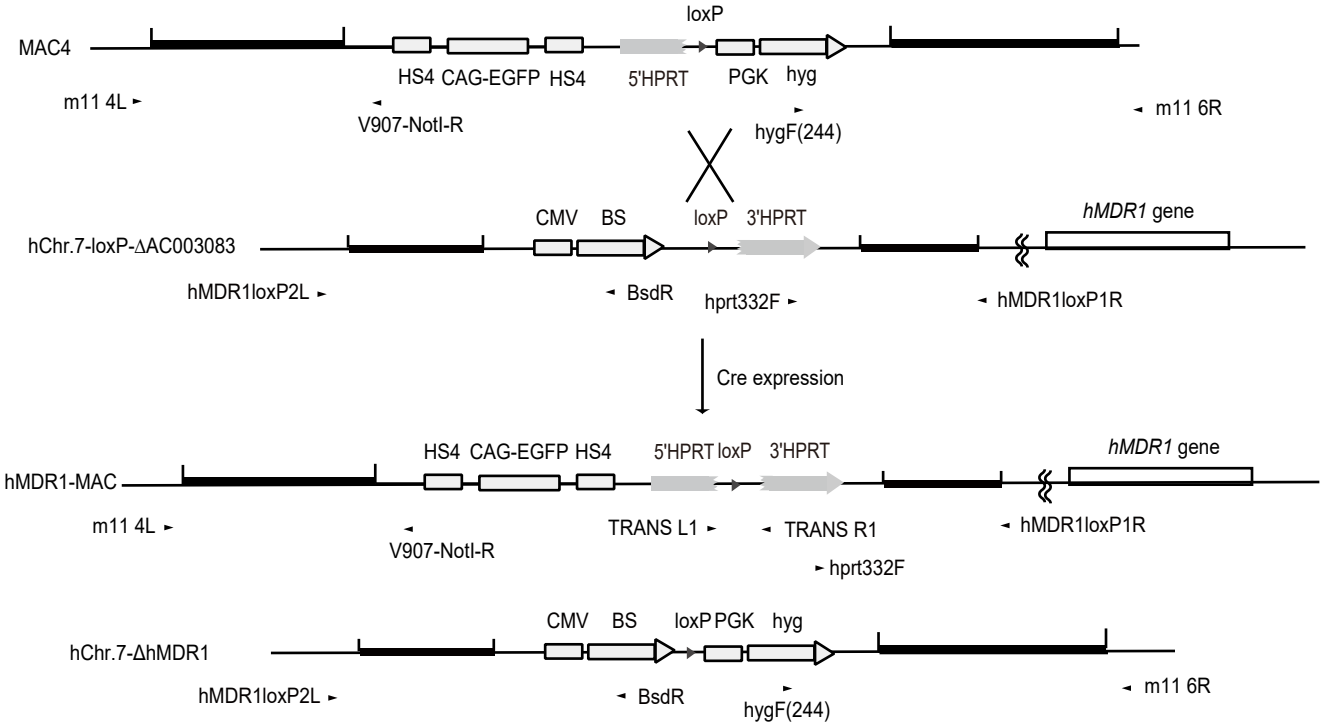

Supplementary Fig. 3. Strategy for Cre/loxP-mediated reciprocal translocation cloning of hMDR1 to MAC4.

MAC4 and the loxP-inserted locus on modified hChr.7 are shown at the top. The resultant hMDR1-MAC and by-product after Cre/loxP-mediated reciprocal translocation are shown at the bottom.

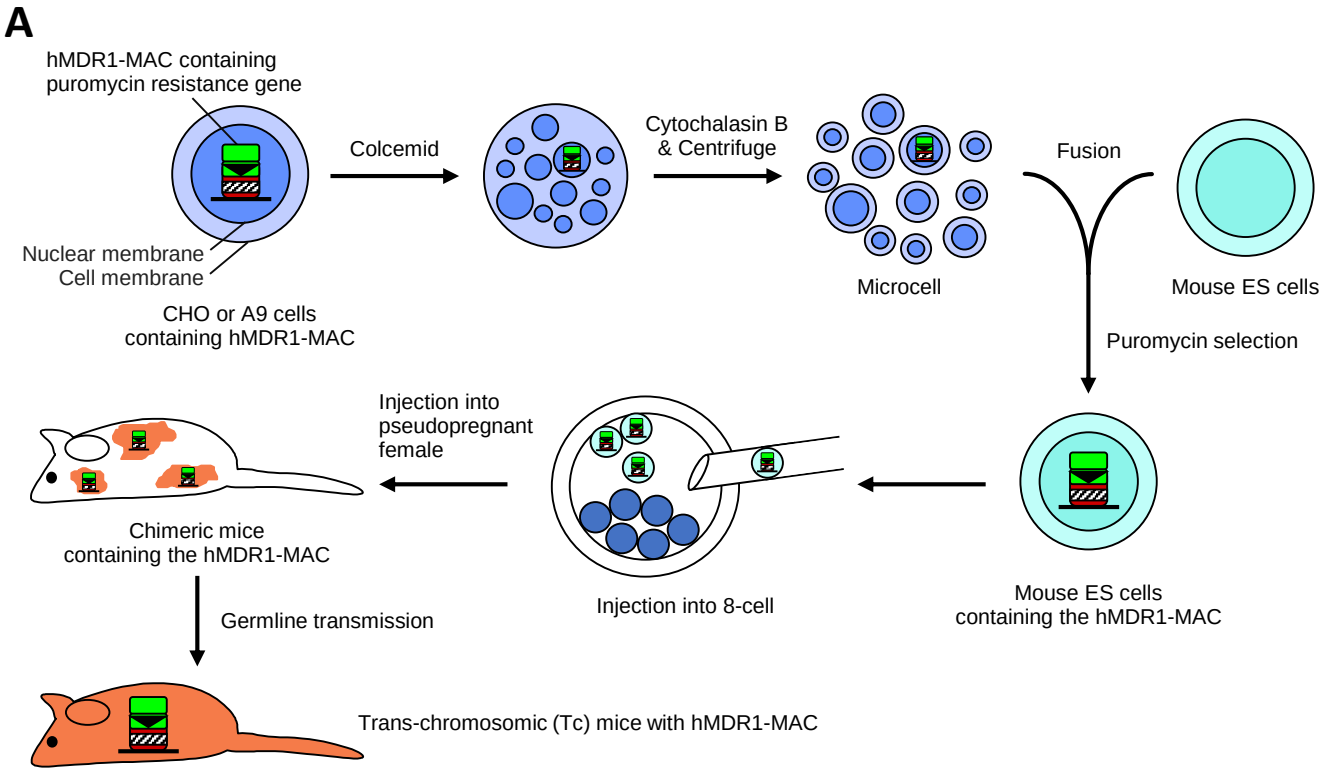

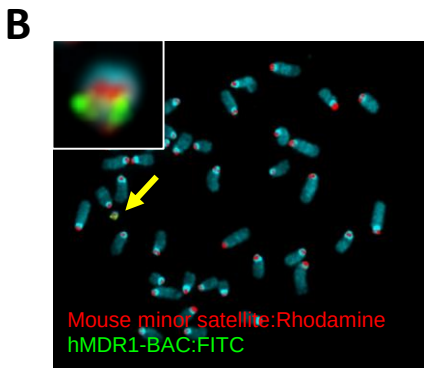

Supplemental Fig. 4. Generation of trans-chromosomic mice with hMDR1-MAC. (A) MMCT of hMDR1-MAC from donor cells to recipient mouse ES cells. (B) FISH image of mouse ES cells containing hMDR1-MAC. Arrows indicate the hMDR1-MAC. Insets show large images of hMDR1-MAC.